

ENVIRONMENTAL DEPENDENCE OF TYPE IA SUPERNOVA LUMINOSITIES FROM THE YONSEI SUPERNOVA CATALOG

YOUNG-LO KIM^{1, 2}, YIJUNG KANG², AND YOUNG-WOOK LEE²

¹Universit de Lyon, F-69622, Lyon, France; Universit de Lyon 1, Villeurbanne; CNRS/IN2P3, Institut de Physique Nuclaire de Lyon; y.kim@ipnl.in2p3.fr

²Center for Galaxy Evolution Research and Department of Astronomy, Yonsei University, Seoul 03722, Korea

Received February 30, 2019; accepted February 31, 2019

Abstract: There is growing evidence for the dependence of Type Ia supernova (SN Ia) luminosities on their environments. While the impact of this trend on estimating cosmological parameters is widely acknowledged, the origin of this correlation is still under debate. In order to explore this problem, we first construct the YONSEI (YOnsei Nearby Supernova Evolution Investigation) SN catalog. The catalog consists of 1231 spectroscopically confirmed SNe Ia over a wide redshift range ($0.01 < z < 1.37$) from various SN surveys and includes the light-curve fit data from two independent light-curve fitters of SALT2 and MLCS2k2. For a sample of 674 host galaxies, we use the stellar mass and the star formation rate data in [Kim et al. \(2018\)](#). We find that SNe Ia in low-mass and star-forming host galaxies are 0.062 ± 0.009 mag and 0.057 ± 0.010 mag fainter than those in high-mass and passive hosts, after light-curve corrections with SALT2 and MLCS2k2, respectively. When only local environments of SNe Ia (e.g., locally star-forming and locally passive) are considered, this luminosity difference increases to 0.081 ± 0.018 mag for SALT2 and 0.072 ± 0.018 mag for MLCS2k2. Considering the significant difference in the mean stellar population age between the two environments, this result suggests that the origin of environmental dependence is most likely the luminosity evolution of SNe Ia with redshift.

Key words: cosmology: observations — distance scale — supernovae: general

1. INTRODUCTION

Observations of distant Type Ia supernovae (SNe Ia) reveal the accelerating expansion of the universe ([Riess et al. 1998](#); [Perlmutter et al. 1999](#)). The use of SNe Ia as a distance indicator is based on two fundamental ideas. The first idea is that SN Ia luminosities can be empirically standardized ([Phillips 1993](#); [Tripp 1998](#)). This is obtained by empirical light-curve fitters, such as SALT2 ([Guy et al. 2007](#)) and MLCS2k2 ([Jha et al. 2007](#)), that correct observed “brighter-slower” and the “brighter-bluer” relations. From this light-curve standardization, the scatter of SN Ia peak luminosity is reduced from ~ 0.3 mag to ~ 0.14 mag ([Guy et al. 2007](#); [Jha et al. 2007](#)).

The other fundamental idea is that the standardization does not evolve with redshift or SN environment. This idea was initially supported by small samples of SNe Ia and their host galaxies: no clear dependence of SNe Ia luminosity, after light-curve shape and color or extinction corrections, on their host morphology was shown ([Riess et al. 1998](#); [Schmidt et al. 1998](#)). However, more recent studies with larger numbers of SNe Ia have revealed $\sim 2\sigma$ trends between the SN corrected luminosity and host galaxy morphology, such that SNe Ia in early-type galaxies are brighter than those in late-type galaxies, both at low- and high-redshift ranges ([Hicken et al. 2009b](#); [Suzuki et al. 2012](#)).

The trends between the corrected luminosity of

SNe Ia and host galaxy properties are now intensively investigated, empirically ([Gallagher et al. 2008](#); [Kelly et al. 2010](#); [Lampeitl et al. 2010](#); [Sullivan et al. 2010](#); [D’Andrea et al. 2011](#); [Gupta et al. 2011](#); [Childress et al. 2013](#); [Johansson et al. 2013](#); [Pan et al. 2014](#); [Campbell et al. 2016](#); [Wolf et al. 2016](#)) and theoretically ([Höflich et al. 1998](#); [Timmes et al. 2003](#); [Kasen et al. 2009](#)). All these studies conclude that SNe in late-type, star-forming, low-mass, and low-metallicity hosts are ~ 0.1 mag fainter than those in early-type, passive, high-mass, and high-metallicity galaxies. Even in recent studies using the “local” environment at the SN explosion site ([Rigault et al. 2013, 2015, 2018](#); [Jones et al. 2018b](#); [Kim et al. 2018](#); [Roman et al. 2018](#)), they also suggest the same result with the similar size of luminosity difference.

Considering the intrinsic scatter of ~ 0.14 mag on the SN Ia luminosity after “empirical” light-curve corrections, ~ 0.1 mag difference from above host galaxy studies implies that there are “physical” processes of SNe Ia we have not well understood yet, such as the different population of them and/or their explosion mechanisms. It is therefore important to investigate the origin of the environmental dependence of SN Ia luminosities to understand the underlying physics of an SN, which could lead to an SN as a more accurate standard candle. Some studies suggest that this dependence may arise from differing stellar population properties of their progenitor or host galaxy, such as age and metallicity

(Timmes et al. 2003; Kasen et al. 2009; Johansson et al. 2013; Childress et al. 2014; Pan et al. 2014; Kang et al. 2016). However, most of the previous works are limited by the sample size and the redshift range, because they used SNe only found in a specific survey (e.g., SDSS-II SNe survey or SN Legacy survey) and analyzed with one light-curve fitter (especially with SALT2). Therefore, in order to investigate the origin of luminosity difference and the underlying physics in detail, we require combining survey data to increase the sample size. As a part of the YONSEI Nearby SN Evolution Investigation (YONSEI; Kim et al. 2015; Kang et al. 2016) project, here we present the YONSEI SN catalog which includes most of the survey data so far to make the sample of 1231 spectroscopically confirmed SNe Ia and 674 host galaxies and has two independent light-curve fitters of SALT2 and MLCS2k2. From this catalog, we show an extended study for the dependence of SN Ia luminosities on the global and local host properties.

2. CONSTRUCTION OF THE YONSEI SUPERNOVA CATALOG

For the YONSEI project, we have constructed our own SNe Ia catalog. We employed SALT2 and MLCS2k2 light-curve fitters implemented in the SuperNova ANALYSIS software (hereafter SNANA; Kessler et al. 2009b) package version 10_34. From this analysis, we have 1231 SNe Ia over the redshift range of $0.01 \leq z \leq 1.37$, which makes this catalog a superset of all SN Ia surveys adopted in the SNANA package.

2.1. Data Sets

SN Ia light-curve data we analyzed are taken from several surveys compiled in the SNANA package except for the Pan-STARRS SN Ia data (hereafter PS, 146 SNe; Rest et al. 2014). Rest et al. (2014) provides the PS light-curves in the SNANA format, so that we add the PS sample to the SNANA light-curve archive. In SNANA, for the ‘LOWZ’ SNe Ia (see Table 1), we use the JRK07 compilation of SNe collected from Calan/Tololo (29 SNe; Hamuy et al. 1996a,b), CfA1 (22 SNe; Riess et al. 1999a), CfA2 (44 SNe; Jha et al. 2006), and other sources (38 SNe; Jha et al. 2007). We also include CfA3 (185 SNe; Hicken et al. 2009a), CfA4 (94 SNe; Hicken et al. 2012), CSP DR1/2 (hereafter CSP, 85 SNe; Contreras et al. 2010; Stritzinger et al. 2011) for our LOWZ sample. In addition, the full three years SDSS-II SNe survey (hereafter SDSS, 500 SNe; Sako et al. 2018), ESSENCE survey (60 SNe; Miknaitis et al. 2007), the first three years of Supernova Legacy survey (hereafter SNLS, 281 SNe; Guy et al. 2010), and *HST* sample (37 SNe; Riess et al. 2004, 2007) are used for our intermediate- and high-redshift SN samples. In total, 1521 SNe Ia were collected for our light-curve analysis (see Table 2). If there are same SNe from different surveys, we use the SN which has the most observations (see e.g., Rest et al. 2014).

2.2. Light-Curve Analysis

2.2.1. SALT2 and MLCS2k2 Light-Curve Fitters Implemented in the SNANA Package

SNANA package was originally developed for the analysis of SDSS SNe data, and then adopted to simulate and fit the SN Ia light-curves in different surveys and from different telescopes. This package contains a light-curve simulation, a light-curve fitter, and a cosmology fitter for all types of SNe. The primary goal of the SNANA package is to use SNe Ia as distance indicators for the estimation of cosmological parameters. Furthermore, it can also be employed to study the SN rate for the selection efficiency, estimate the non-Ia contamination, and optimize future SN surveys. In the SNANA package, most of the current SN models and non-Ia models are included. For the YONSEI catalog, we employed the most up-to-date SALT2 (version 2.4 from Betoule et al. (2014)) and MLCS2k2 (with $R_V = 2.2$) light-curve fitters. We note that for the MLCS2k2, we select a flat prior allowing negative A_V values, and $R_V = 2.2$ for the dust reddening parameter, which is the same value as in Kessler et al. (2009a).

The purpose of the two light-curve fitters of SALT2 and MLCS2k2 is to determine the luminosity distance of SNe Ia. A basic equation to estimate distances from SNe Ia (μ_{SN}) is parameterized by a linear function of light-curve shape and color or extinction parameters, using the following equation (Tripp 1998):

$$\mu_{SN} = m_B - M_B + \alpha \times (\text{light-curve shape}) - \beta \times (\text{color or extinction}), \quad (1)$$

where m_B is an observed rest-frame peak apparent magnitude in B -band, M_B is an absolute magnitude determined from an SN intrinsic luminosity, and α and β are global parameters that characterize the brighter-slower and brighter-bluer relations, respectively. SALT2 and MLCS2k2 fit each observed light-curve for the peak magnitude, the shape parameter (X_1 for SALT2 and Δ for MLCS2k2), and the color (C for SALT2) or host galaxy extinction value (A_V for MLCS2k2), under an implicit assumption that SNe Ia at low-redshift and those at high-redshift are the same for a given shape and color within the observed scatter. However, these fitters have different ways of estimating model parameters from light-curve data, different approaches to training the models, and different assumptions about the treatment of color variations in SNe Ia. Although SALT2 is the most widely used light-curve fitter in the SN community, MLCS2k2 has a novelty in the context of the investigation of the luminosity evolution of SNe Ia. SALT2 is calibrated by using SNe spanning from the low- to the high-redshift range, while MLCS2k2 is calibrated based solely on SNe at low-redshift (see e.g., Guy et al. 2010; Betoule et al. 2014; Jones et al. 2015). At high redshift, young progenitors might be dominant, while young and old progenitors are expected to be mixed at low redshift. Therefore, in SALT2, the possible luminosity evolution effect is more diluted than that

Table 1
Contributions to the LOWZ Sample in the YONSEI SN Catalog

SN Data	Redshift Range	Total	SALT2		MLCS2k2	
			Cosmology Sample	All Sample	Cosmology Sample	All Sample
JRK07	0.01-0.09	133	59	69	46	69
CFA3	0.01-0.07	185	73	89	62	96
CFA4	0.01-0.08	94	46	59	35	66
CSP	0.01-0.09	85	40	49	31	62
LOWZ	0.01-0.09	497	218	266	174	293

Table 2
Contributions and Cuts for Each Sample in the YONSEI SN Catalog

Light-Curve Fitter	SN Data	Redshift Range	Total	Final (=Cosmology sample)	Initial Cut (=All sample)	Cosmology Cut	Chauvenet's Criterion
SALT2	YONSEI	0.01-1.37	1521	1049	339	129	4
	LOWZ	0.01-0.09	497	218	231	45	3
	SDSS	0.03-0.41	500	392	64	43	1
	PS	0.03-0.64	146	108	23	15	0
	ESSENCE	0.15-0.70	60	51	0	9	0
	SNLS	0.12-1.06	281	262	9	10	0
	HST	0.21-1.37	37	18	12	7	0
MLCS2k2	YONSEI	0.01-1.37	1521	821	333	362	5
	LOWZ	0.01-0.09	497	174	204	116	3
	SDSS	0.03-0.41	500	328	82	90	0
	PS	0.03-0.64	146	98	21	27	0
	ESSENCE	0.15-0.70	60	41	1	18	0
	SNLS	0.12-1.06	281	170	9	100	2
	HST	0.21-1.37	37	10	16	11	0

in MLCS2k2. In this respect, MLCS2k2 could be more powerful to reveal the luminosity evolution of SNe Ia. In this paper, which also explores the possible luminosity evolution of SNe Ia, we hence use both fitters and analyze them separately, and then compare the results.

2.2.2. Initial Cut Criteria

The 1521 SN light-curve data we collected were analyzed by SALT2 and MLCS2k2 fitters with the initial cut criteria. The initial criteria are based on 1) the light-curve data quality, 2) the light-curve fit quality, and 3) the redshift, which are similar to the criteria adopted in [Betoule et al. \(2014\)](#), [Rest et al. \(2014\)](#), and [Sako et al. \(2018\)](#). Of the 1521 SNe, 1182 for SALT2 and 1188 for MLCS2k2 pass this requirement. We detail the selection criteria below and the number of cuts in each data set is listed in [Table 2](#).

Light-curve data quality criteria:

- 1-1) at least 1 measurement with $-20 \text{ days} < t < +10 \text{ days}$, where t is the rest-frame phase relative to the time of maximum light in B -band.
- 1-2) at least 1 measurement with $+0 \text{ days} < t < +50 \text{ days}$.
- 1-3) at least 3 measurements between $20 \text{ days} < t < +50 \text{ days}$.
- 1-4) 2 or more filters with signal-to-noise ratio ≥ 3 .

Light-curve fit quality and the redshift criteria:

- 2-1) $P_{fit} \geq 0.01$, where P_{fit} is the SNANA light-curve fit probability based on the χ^2 per degree of freedom.
- 2-2) Visual inspection for the SN light-curve fit.
- 3-1) $z \geq 0.01$, in order to include SNe Ia in the Hubble flow.

[Conley et al. \(2011\)](#) pointed out that the cut using an automated quality of fit based on χ^2 statistics (e.g., P_{fit}) is often misleading, especially for the LOWZ sample. Many SNe in the LOWZ sample have the occasional outlying measurements which have little or no effect on the light-curve fitting, but derive a large value of χ^2 of the fit. In order to prevent this situation, we therefore have performed a visual inspection, together with the value of P_{fit} , to check the light-curve fit quality.

2.2.3. Bias Correction and Error Analysis

Before we determine the best-fit cosmological parameters from our sample, we should first consider the selection bias and the uncertainties in distance modulus. SN samples from flux-limited surveys are affected by the Malmquist bias ([Malmquist 1936](#)) or the selection bias: intrinsically brighter and more slowly declining SNe Ia would less suffer from the selection effect

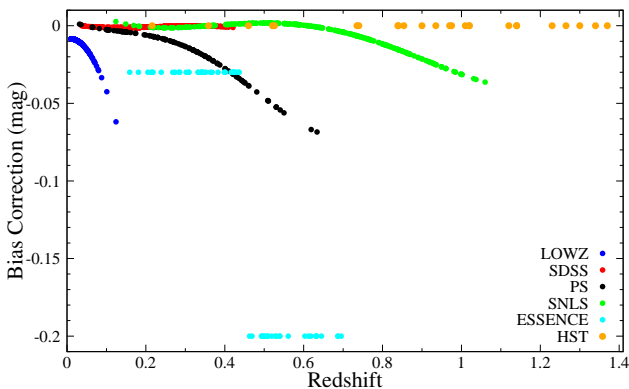


Figure 1. Bias correction for each SN in the YONSEI SN Catalog as a function of redshift. We subtracted this value from all of the rest-frame peak magnitudes in B -band for SALT2 and all of the distance modulus for MLCS2k2 in our sample.

and stay longer above the detection threshold than intrinsically fainter and fast declining SNe, and hence be easier to observe. This leads to creating a false result of increasing luminosity of SNe Ia at a given distance. Consequently, the bias has an effect on the estimating distance, such that the determined SN luminosity distance might be closer than the true value. Therefore, we should correct the Malmquist bias to obtain accurate cosmological parameters. Since the effect of the bias differs from survey to survey, we need to explicitly correct it for our analysis according to each survey. We take correction terms for LOWZ, SDSS, and SNLS samples from those calculated by [Betoule et al. \(2014\)](#), which has a very similar sample to our catalog. For the PS sample, we take the term from [Rest et al. \(2014\)](#), and from [Wood-Vasey et al. \(2007\)](#) for the ESSENCE sample. As [Strolger et al. \(2004\)](#) argued that the HST searches are sufficiently deep to suffer from little or no Malmquist bias out to the maximum redshift where SN discovered, we do not perform the bias correction for the HST sample (see also [Conley et al. 2011](#)). We then interpolate the correction value for each SN at a given redshift (Figure 1), and this value is subtracted from all of the rest-frame peak magnitudes in the B -band for SALT2 and all of the distance moduli for MLCS2k2 in our catalog.

The total uncertainty is generally computed by the propagation of statistical and systematic uncertainties. The systematic uncertainties are associated with the calibration, the light-curve model uncertainty, the host dependency, and so on. In this paper, our purpose is to investigate one of the systematic uncertainties, the host dependency, so here we consider only the statistical uncertainties.

Following [Conley et al. \(2011\)](#) and [Betoule et al. \(2014\)](#), the (statistical) uncertainty for each SN is propagated in the polynomial form given by

$$\sigma_{stat}^2 = \sigma_{fit}^2 + \sigma_z^2 + \sigma_{lens}^2 + \sigma_{int}^2, \quad (2)$$

where σ_{fit} is the error on the fitted light-curve param-

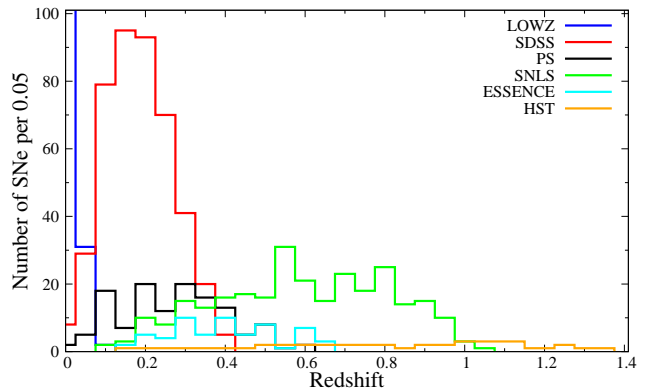


Figure 2. Redshift distribution of the YONSEI All sample. Histograms are colored by surveys. The first bin of the LOWZ sample contains 268 SNe Ia.

eters estimated from SALT2 and MLCS2k2, σ_z accounts for the redshift determination uncertainty, σ_{lens} represents the statistical variation of magnitudes caused by the gravitational lensing, and σ_{int} is the intrinsic scatter of SNe Ia to make a reduced χ^2 (χ_{red}^2 ; the χ^2 per degree of freedom) a unity when we determine the best-fit cosmology. Our approximation of the redshift uncertainty follows Equation (5) of [Conley et al. \(2011\)](#), and the random, uncorrelated scatter due to the lensing follows the suggestion of [Jönsson et al. \(2010\)](#): $\sigma_{lens} = 0.055 \times z$. The intrinsic scatter is not included in our analysis, as we are searching this extra scatter through the systematic variation in SN Ia luminosity on the host galaxy properties ([D’Andrea et al. 2011](#); [Gupta et al. 2011](#); [Pan et al. 2014](#)).

2.3. YONSEI Supernova Catalog and Systematic Tests

After applying the bias correction and the error propagation for the uncertainty, now we have the YONSEI SN Catalog (see Table 3). This catalog provides a rest-frame peak magnitude in B -band or distance modulus, a light-curve shape parameter, and a color or host extinction value for each SN. Because both normal and peculiar SNe Ia are included, we call this catalog as the YONSEI ‘All’ sample to distinguish from the YONSEI ‘Cosmology’ sample which only has normal SNe described in next Section. The redshift distribution of the YONSEI All sample is shown in Figure 2.

In order to look for the systematic trends for both fitters and SN samples we employed, we analyze the output of the YONSEI SN Catalog. From this analysis, we would provide light-curve fit parameter areas for the study of the SN cosmology (the cosmology cut) and also examine the consistency between fitters as pointed out by previous studies.

2.3.1. Light-Curve Shape and Color or Extinction Values as a Function of Redshift

In Figures 3 and 4, we show the distributions of fitted shape and color or host extinction values of SALT2 and MLCS2k2 as a function of redshift, respectively. At the higher redshift range, both faint and red or highly

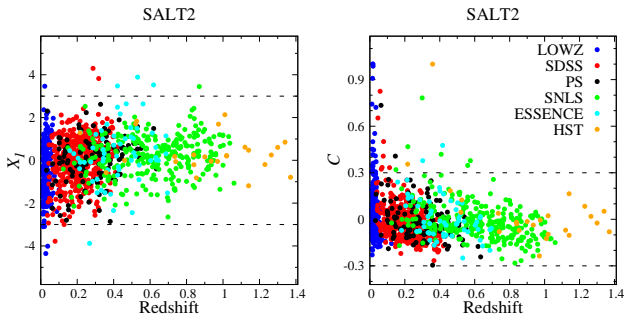


Figure 3. Distribution of SALT2 fit parameters in the YONSEI All sample: X_1 (left panel) and C (right panel) versus redshift. Faint (low X_1) and red (high C) SNe Ia are not found at the higher redshift range. SNe are colored by surveys. The dashed lines indicate our cosmology cut criteria we employed for SALT2 ($-3 < X_1 < 3$ and $-0.3 < C < 0.3$).

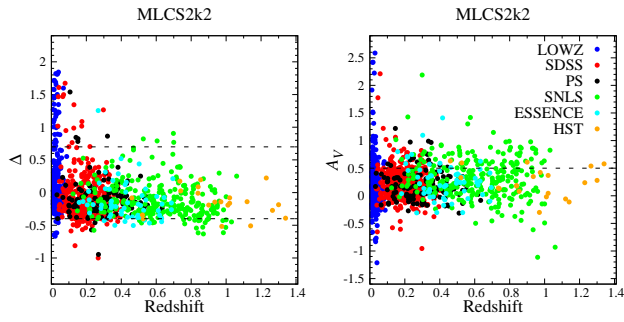


Figure 4. Same as Figure 3, but for MLCS2k2 fit parameters: Δ (left panel) and A_V (right panel). Faint (high Δ) and highly reddened (high A_V) SNe Ia are not found at the higher redshift range. The dashed lines indicate our cosmology cut criteria we employed for MLCS2k2 ($-0.4 < \Delta < 0.7$ and $A_V < 0.5$).

reddened SNe Ia are not found. However, it is unclear whether this is because of the magnitude-limited surveys or the luminosity evolution of SNe Ia with redshift. We note that since we select the flat prior allowing negative A_V values for our MLCS2k2 extinction distribution prior (see Section 2.1), there are many SNe with $A_V < 0$ on the right panel in Figure 4. However, the negative- A_V distribution has little effect on the Δ distribution (Kessler et al. 2009a).

Considering the SNe Ia at the higher redshift range and the criteria adopted in Betoule et al. (2014) and Hicken et al. (2009b), here we preliminarily define one of our cosmology cut criteria (see Section 2.4.1). For SALT2, we employ $-3 < X_1 < 3$ and $-0.3 < C < 0.3$, and for MLCS2k2 we select $-0.4 < \Delta < 0.7$ and $A_V < 0.5$. As shown in Figures 3 and 4, most of SNe at the higher redshift range are included, except highly reddened ones in MLCS2k2.

2.3.2. Comparison between SALT2 and MLCS2k2 Light-Curve Fit Parameters

Next, we compare the light-curve fit parameters between SALT2 and MLCS2k2 to examine the consistency

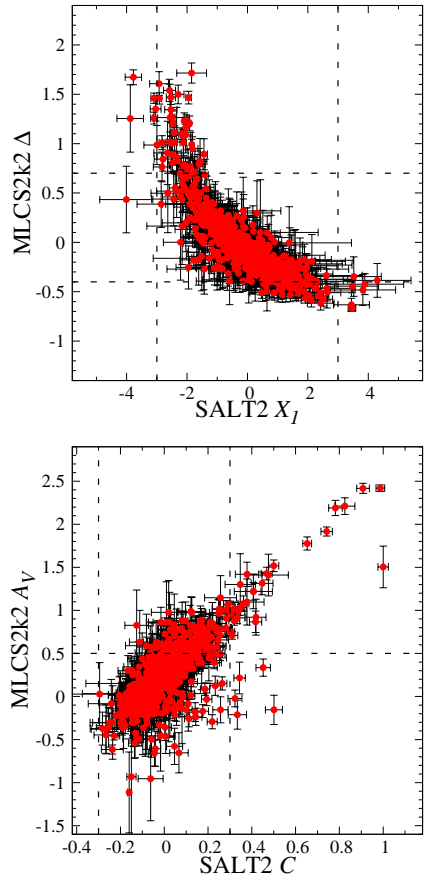


Figure 5. Comparison between SALT2 and MLCS2k2 light-curve fit parameters. The upper panel shows the comparison of light-curve shape parameters, SALT2 X_1 versus MLCS2k2 Δ , and the reddening parameters, SALT2 C versus MLCS2k2 A_V , are compared in the lower panel. There is a good correlation between each other, as presented by Hicken et al. (2009b) and Sako et al. (2018). The dashed lines indicate our cosmology cut criteria for both fitters, and many outliers are discarded from these criteria.

with each other. In Figure 5, SALT2 X_1 is compared to MLCS2k2 Δ in the upper panel, and SALT2 C is compared to MLCS2k2 A_V in the lower panel. There is a good correlation between SALT2 and MLCS2k2 fit parameters, with a scatter and some outliers. X_1 and Δ are nonlinearly correlated, while C and A_V are linearly correlated, as presented by Hicken et al. (2009b) and Sako et al. (2018). As shape parameters show nonlinearity, Δ spans a wide range in the vicinity of $X_1 = -2$ (fast-declining), and the brightest SNe (negative Δ) also have a wide range of X_1 . Our cosmology cut criteria indicated by dashed lines exclude most of SNe in this nonlinear region. We note that there is a zeropoint offset for the color between the fitters, $C \approx -0.1$ when $A_V = 0$. Overall, light-curve fit parameters of SALT2 and MLCS2k2 we obtained show a good agreement between the two.

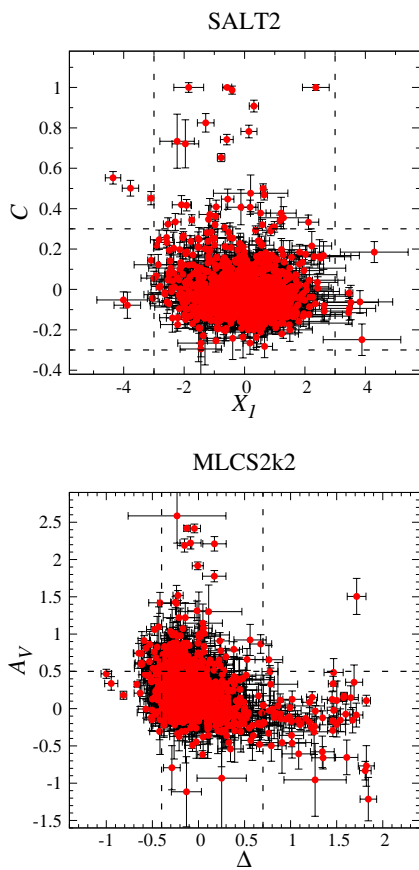


Figure 6. Distribution of shape and color or host extinction values for SALT2 (upper panel) and MLCS2k2 (lower panel). We expect that peculiar SNe Ia are mostly placed in the scattered region. The dashed lines indicate our cosmology cut criteria, and most of peculiar SNe are removed by these cuts.

2.3.3. Distribution of Shape and Color or Extinction Values for SALT2 and MLCS2k2

Finally, we show the distribution of shape and color or host extinction values for SALT2 and MLCS2k2 in Figure 6 to investigate the systematic trends in the YONSEI All sample. From the definition of the fitters, SNe Ia form a well-defined cluster of points centered on zero in the parameter space (e.g., Campbell et al. 2013). We expect that peculiar SNe Ia are mostly placed in the scattered region. As shown in the figure, our cosmology cut criteria we employed discard most of the scattered (i.e., peculiar) SNe Ia.

2.4. YONSEI Hubble–Lemâitre Diagram

2.4.1. YONSEI Cosmology Sample

In order to estimate the best-fit cosmological parameters, we should consider selecting only well-fitted normal SNe Ia from the YONSEI All sample compiled above. For this (the YONSEI ‘Cosmology’ sample), we require the cosmology cut criteria. Following the criteria investigated in the previous section and adopted in Betoule et al. (2014) and Hicken et al.

(2009b), the cuts are based on the 1) the Milky Way extinction, 2) the uncertainty on the time of maximum in B -band (t_0), 3) the uncertainty on the light-curve shape parameter, and 4) the fitted shape and color or extinction parameters of each light-curve fitter. We detail the criteria below and the number of cosmology cuts is listed in Table 2.

Cosmology cut criteria:

- 1) $E(B - V)_{MW} < 0.15$ mag.
- 2) $\sigma(t_0) < 2$.
- 3) $\sigma(shape) < 1$.
- 4) $-3 < X_1 < 3$ and $-0.3 < C < 0.3$ for SALT2, and $-0.4 < \Delta < 0.7$ and $A_V < 0.5$ for MLCS2k2.

We then use the JLA likelihood code (Betoule et al. 2014) to estimate the best-fit cosmological parameters for the YONSEI Cosmology sample assuming the flat Λ CDM model. The best-fit cosmological parameters obtained for our main cosmology sample were $\Omega_M = 0.30$, $\alpha = 0.15$, $\beta = 3.69$, and $M_B = -19.06$ for SALT2, and $H_0 = 63$ and $\Omega_M = 0.43$ for MLCS2k2¹. During estimating cosmological parameters, we applied Chauvenet’s criterion (Taylor 1997) to reject outliers, removing SNe whose probability of obtaining a deviation from a mean is less than $1/(2 \times \text{sample size})$, assuming a Gaussian distribution of intrinsic luminosities. For our samples, this corresponds to 3.5σ for SALT2 and 3.4σ for MLCS2k2. This criterion does not significantly depend on the choice of cosmological models, and therefore the same SNe are excluded for all choices. The number of cuts by Chauvenet’s criterion is listed in Table 2. Finally, of the 1182 SNe, 1049 pass the cosmology cut and Chauvenet’s requirement for SALT2, and of the 1188 SNe, 821 pass for MLCS2k2.

2.4.2. Hubble–Lemâitre Diagram for the YONSEI Cosmology Sample

From the YONSEI Cosmology sample and best-fit cosmological parameters we obtained above, finally, here we present the YONSEI Hubble–Lemâitre diagram in Figures 7 and 8 for SALT2 and MLCS2k2, respectively. Hubble residuals (HRs $\equiv \mu_{SN} - \mu_{model}(z)$, where $\mu_{model}(z)$ is the predicted distance modulus based on the cosmological model) from the best-fit are also presented in the bottom panel.

Table 4 shows the weighted means and rms scatters of the HRs for each data set. The average weighted mean of the YONSEI Cosmology sample is 0.00 ± 0.01 mag, and the average rms scatter is ~ 0.19 mag. When we look at the table by data sets, the HST sample has a more negative weighted mean of HRs than other samples. This means that the HST sample is brighter, after light-curve corrections, than samples in other surveys. However, as discussed in Section 2.3.1, it is not clear

¹This is most likely due to the lack of recent calibration of MLCS2k2 by using the SNe Ia at the high-redshift range (see e.g., Guy et al. 2010; Betoule et al. 2014; Jones et al. 2015).

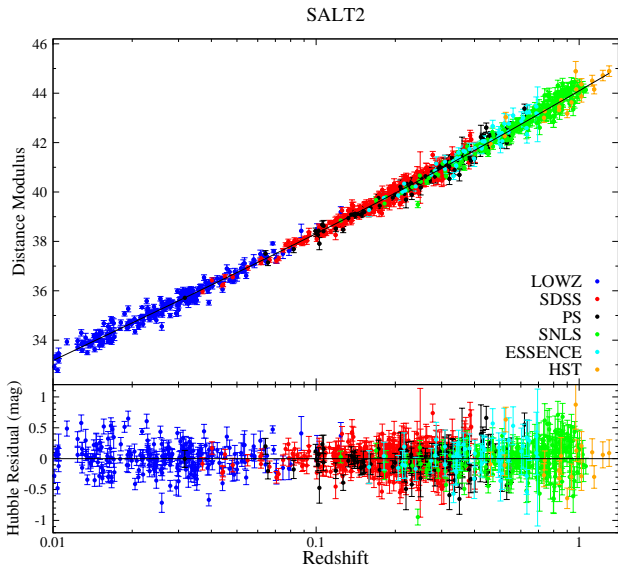


Figure 7. YONSEI Hubble–Lemaitre diagram and residuals for the SALT2 sample. The solid line represents the best-fit flat Λ CDM cosmology parameters for SNe Ia alone. The values we obtained are $\Omega_M = 0.30$, $\alpha = 0.15$, $\beta = 3.69$, and $M_B = -19.06$. HRs from the best-fit are shown in the bottom panel. SNe are colored by surveys.

whether this is due to the selection bias or intrinsic differences in SNe Ia. Because of the larger photometric uncertainties, the HST and ESSENCE samples show larger values in the rms scatter. However, our rms values for both samples are similar to those in previous studies (see the rms values for the high- z sample in Hicken et al. 2009b; Kessler et al. 2009a; Conley et al. 2011; Suzuki et al. 2012).

2.4.3. Systematic Tests for Hubble Residuals

We now turn to find out systematic trends in HRs, because these trends, if any, could give an effect on our results described in the following sections. In Figure 9, we first present a correlation between the HRs obtained from SALT2 and MLCS2k2 fitters. They show a good agreement with a mean offset of 0.02 mag and the correlation coefficient of 0.86. As we show that SALT2 and MLCS2k2 are similarly characterizing the SN Ia light-curves (see Section 2.3.2), most of the residual scatters might be due to the different methods they used when both fitters are determining the distance modulus.

Figure 10 shows HRs as a function of the light-curve shape parameters for SALT2 and MLCS2k2, respectively. No significant trends are found for both fitters. Outliers (cross marks), which are expected to be peculiar SNe Ia, are appropriately removed by our cosmology cut criteria (dashed lines). We note a peculiar region in the lower panel. In the region of $\Delta > 0.7$ for MLCS2k2, the residuals have mostly negative values as pointed out by Hicken et al. (2009b). They discussed that this “dip” is most likely due to 1991-bg like SNe Ia, which are fainter than normal SNe Ia. However, this class of SNe is also well discarded by our cosmology cut

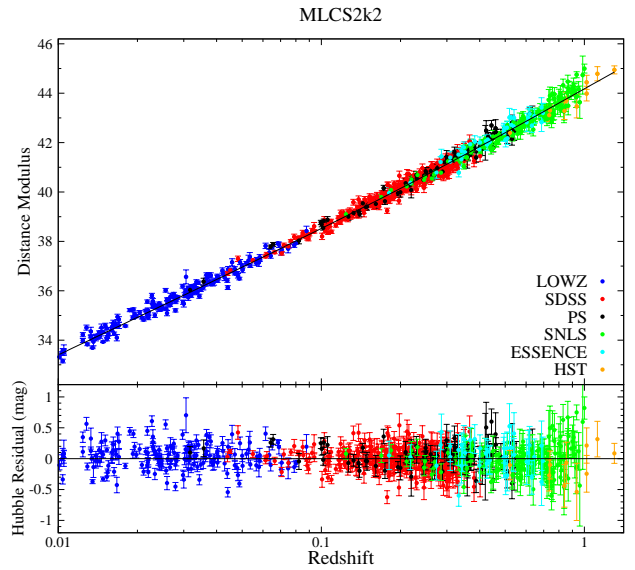


Figure 8. Same as Figure 7, but for the MLCS2k2 sample. Best-fit flat Λ CDM cosmology parameters we obtained are $H_0 = 63$ and $\Omega_M = 0.43$.

criteria.

Finally, we plot the HRs versus C and A_V for SALT2 and MLCS2k2 in Figure 11. At first sight, it looks like that there are negative trends between HRs and C or A_V for both fitters. Even though the redder ($C > 0.3$ for SALT2) and highly reddened ($A_V > 0.5$ for MLCS2k2) SNe, which have mostly negative residuals, are removed by our cosmology cut criteria, trends still remain. In order to investigate this, we have plotted the HRs versus C and A_V for SALT2 and MLCS2k2 with a sample split by redshift range in Figures 12 and 13, respectively. As shown in the figures, the negative trends are universal at all samples in the different redshift ranges. However, Hicken et al. (2009b) showed that the cuts on C and A_V make this trend have little effect on the SN cosmology. On the other hand, we could consider that this trend would show a hint of the dependence of SN luminosities on host galaxies. For example, hosts which have highly reddened SNe might be related to star-forming environments (young populations), while those with little extinction values are related to passive environments (old populations).

2.5. Host Galaxy Data

Host galaxy properties, specifically morphological types, the stellar mass (M_{stellar}), and global specific star formation rate ($sSFR$; the star formation rate per unit stellar mass), are also required to explore the environmental dependence of SN Ia luminosities. Morphological types for the LOWZ sample (194 SNe out of 218) are drawn from the NASA Extragalactic Database (NED)² and the HyperLeda database (Makarov et al. 2014)³, and from the Korea Institute for Advanced Science Value-Added Galaxy Catalog (Choi et al. 2010,

²<http://ned.ipac.caltech.edu/>

³<http://leda.univ-lyon1.fr/>

Table 4
The Weighted Mean and rms Scatter of Hubble Residuals in Each Data Set

SN Data	SALT2					MLCS2k2				
	N_{SN}	HR_{WM} (mag)	Error (mag)	rms (mag)	Error (mag)	N_{SN}	HR_{WM} (mag)	Error (mag)	rms (mag)	Error (mag)
YONSEI	1049	0.000	0.006	0.194	0.004	821	0.006	0.006	0.182	0.004
LOWZ	218	0.020	0.015	0.206	0.010	174	0.011	0.015	0.188	0.010
SDSS	392	-0.006	0.008	0.165	0.006	328	-0.003	0.008	0.153	0.006
PS	108	-0.022	0.017	0.172	0.012	98	0.056	0.016	0.156	0.011
ESSENCE	51	0.016	0.033	0.235	0.023	41	0.049	0.036	0.230	0.026
SNLS	262	-0.006	0.012	0.197	0.009	170	-0.014	0.015	0.191	0.010
HST	18	-0.116	0.069	0.294	0.051	10	-0.054	0.072	0.227	0.053

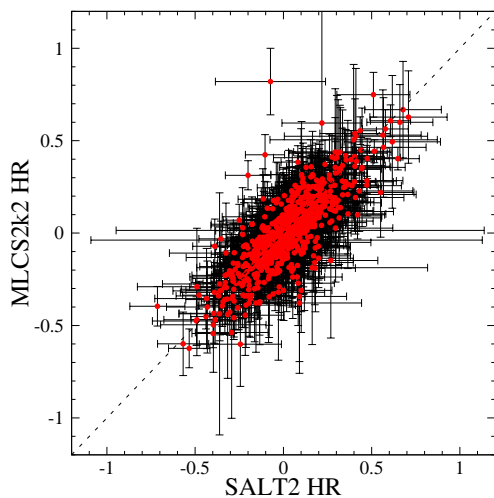


Figure 9. Correlation between HRs obtained from SALT2 and MLCS2k2. They show a good agreement with a mean offset of 0.02 mag, and the value of the correlation coefficient is 0.86. 718 SNe Ia are cross-matched on SALT2 and MLCS2k2. There is an outlier, 06D2cb in the SNLS sample, for which only one filter is used when MLCS2k2 estimates light-curve fit parameters. The dashed line is for the one-to-one relation.

KIAS-VAGC)⁴ and Han et al. (2010) for the SDSS sample (55 out of 392).

Host $M_{stellar}$ and global $sSFR$ are taken from Kim et al. (2018), which provide the host data for LOWZ, SDSS, and SNLS samples⁵. Briefly, they employ the PÉGASE.2 galaxy spectral evolution code (Fioc & Rocca-Volmerange 1997; Le Borgne & Rocca-Volmerange 2002; Le Borgne et al. 2004) to determine host galaxy properties, following the method described in detail in Sullivan et al. (2006, 2010). They use a set of 14 exponentially declining star formation histories (SFHs) and foreground dust screens ranging from $E(B - V) = 0$ to 0.30 mag in steps of 0.05. Then, they fit the host galaxy data from Smith et al. (2012) and Sako et al. (2018) (for the SDSS sample), and Sullivan et al. (2010) (for the SNLS sample). Host galaxy prop-

⁴<http://astro.kias.re.kr/vagc/dr7/>

⁵Since Kim et al. (2018) do not provide the host data for PS, ESSENCE, and HST samples, we do not include those samples in our host analysis.

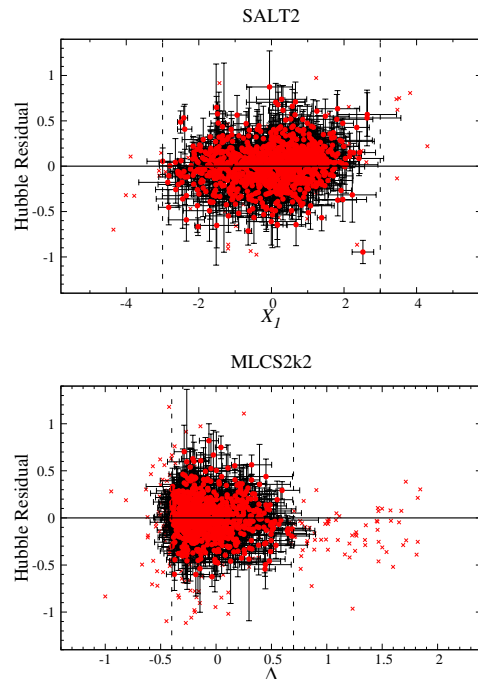


Figure 10. HRs versus light-curve shape parameters for SALT2 (X_1 ; upper panel) and MLCS2k2 (Δ ; lower panel). No significant trends exist for both fitters. Outliers (mostly peculiar SNe Ia; cross marks) are appropriately removed by our cosmology cut criteria (dashed lines). Note a peculiar region ($\Delta > 0.7$) in the lower panel, where SNe have mostly negative HR values. These 1991bg-like SNe Ia are also well removed by our cosmology cut criteria.

erties for the LOWZ sample are taken from Neill et al. (2009) that uses the same PÉGASE.2 approach. In total, for SALT2, 89 (out of 218) for LOWZ, 355 (out of 392) for SDSS, and 213 (out of 262) hosts for SNLS are matched with the YONSEI Cosmology sample, while for MLCS2k2, 73 (out of 174) for LOWZ, 292 (out of 328) for SDSS, and 147 (out of 170) hosts for SNLS are collected. The data and sample sizes used in our analysis are listed in Tables 3 and 5, respectively. We note that as mentioned in Sullivan et al. (2010) and Kim et al. (2018), we also restrict the SNLS sample to $z \leq 0.85$, where the SNLS sample has the highest signal-to-noise ratio and the Malmquist corrections are the smallest.

Figures 14 and 15 show the distributions of the

Table 5
Summary of Host Data in the YONSEI SN Catalog

SN Data	SALT2				MLCS2k2			
	N_{SN}	Morphology	Mass & sSFR	Local Environment	N_{SN}	Morphology	Mass & sSFR	Local Environment
LOWZ	218	194	89	40	174	152	73	29
SDSS	392	55	355	203	328	45	292	164
SNLS	262	0	213	130	170	0	147	96
YONSEI	872	249	657	373	672	197	512	289

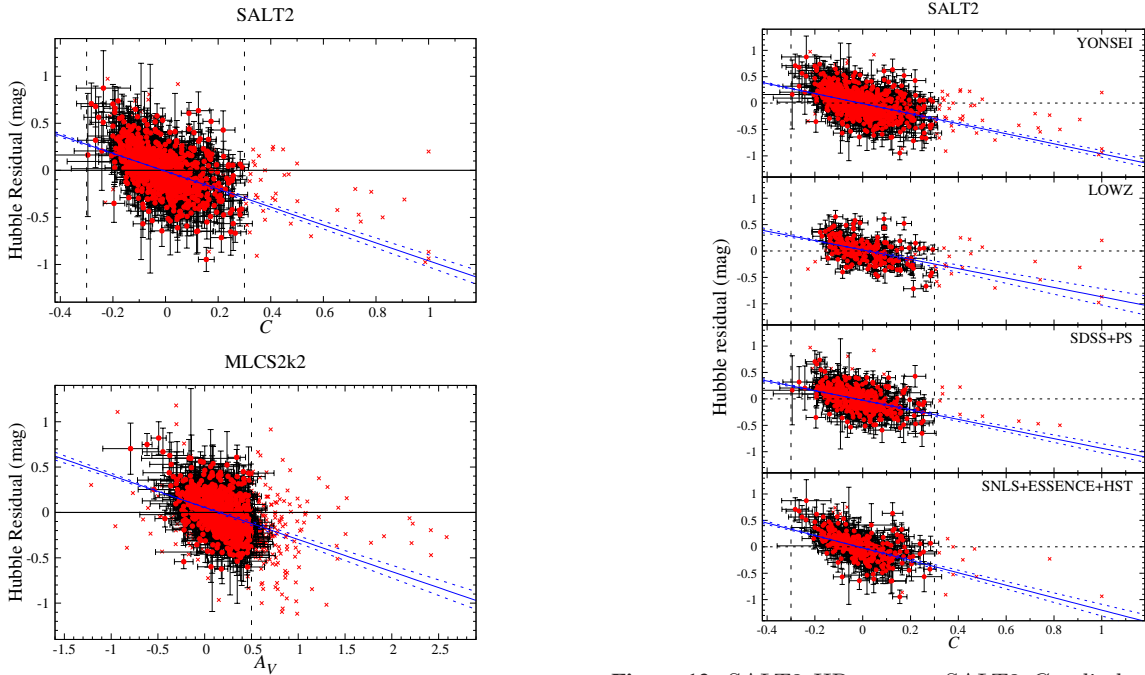


Figure 11. HRs versus C and A_V for SALT2 (upper panel) and MLCS2k2 (lower panel). Most of SNe Ia are well-clustered, but there are negative trends in both fitters (blue lines with $\pm 1\sigma$ ranges). The black dashed lines indicate our cosmology cut criteria. The redder ($C > 0.3$ for SALT2) and highly reddened ($A_V > 0.5$ for MLCS2k2) SNe, which have mostly negative residuals, are removed by these cut criteria.

YONSEI host sample in the host galaxy morphology, $M_{stellar}$, and $sSFR$ planes. As shown in the figures, SNe Ia prefer to explode in the late-type, star-forming, and more massive (high-mass; $\log(M_{stellar}) > 10.0$) systems. We note that the fraction of high-mass hosts in the LOWZ sample is much higher than that in other samples (see the blue histogram in the upper panel of Figure 15). This is because many SNe in the LOWZ sample were discovered in host-targeted surveys which prefer more luminous and massive galaxies, while the SDSS and SNLS samples were from untargeted rolling surveys without selection biases (see also Neill et al. 2009; Kelly et al. 2010; Sullivan et al. 2010; Pan et al. 2014). In $sSFR$, the distributions of each sample (the lower panel of Figure 15) are fairly similar, as pointed out by Neill et al. (2009).

Figure 12. SALT2 HRs versus SALT2 C split by SN data. Negative trends are observed in every sample (blue lines with $\pm 1\sigma$ ranges).

We have also investigated the distribution of our host galaxies in the $M_{stellar}$ – $sSFR$ plane in Figure 16. We see that most of the high-mass host galaxies have a lower value of $sSFR$, while the low-mass hosts universally show a strong star formation activity, as expected.

Finally, we note that in the following sections, we will investigate the dependence of various SN Ia properties on their host galaxy properties. Therefore, we need to split the host galaxies into several different groups. The first group is split according to their morphology: early- and late-types. In the case of the LOWZ sample, we further split it more specifically as E–S0, S0a–Sc, and Scd/Sd/Irr galaxies, following the scheme presented in Hicken et al. (2009b). The second group is split into high- and low-mass galaxies by a value of $\log(M_{stellar}) = 10.0$ (the black vertical line in Figure 16; see Sullivan et al. 2010; Childress et al. 2013; Pan et al. 2014). The final group is split based on the $\log(sSFR)$: passive and star-forming environments split at $\log(sSFR) = -10.4$ (the black horizontal line in Figure 16; for the similar criteria, see Sullivan et al. 2010; Childress et al. 2013; Rigault et al. 2013, 2015;

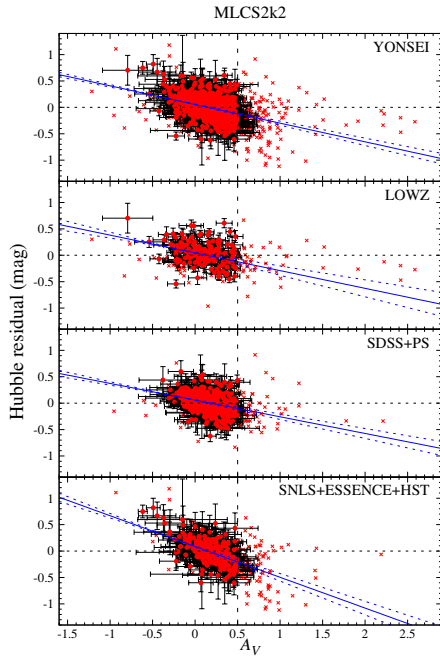


Figure 13. Same as Figure 12, but for MLCS2k2 A_V . We observe a negative trend in every sample (blue lines with $\pm 1\sigma$ ranges).

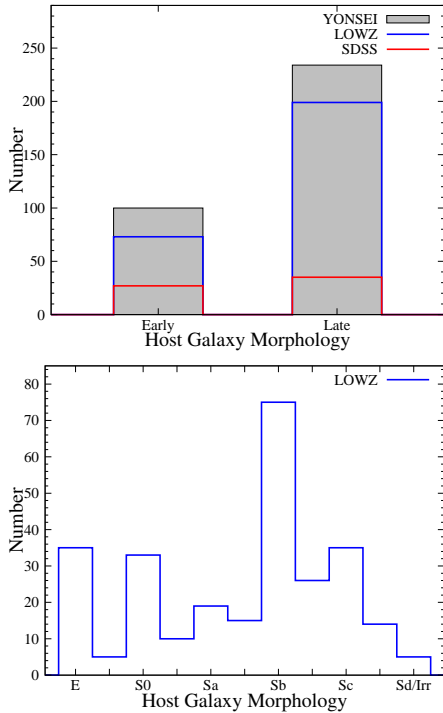


Figure 14. Distribution of the YONSEI host sample in the host galaxy morphology. Only LOWZ (blue histogram) and SDSS (red histogram) samples have host morphological information (see text). The upper panel shows the distribution of those samples when we divide hosts as early- and late-type galaxies, and the lower panel is only for the LOWZ sample with more specific morphological types. SNe Ia prefer to explode in the late-type galaxies as expected.

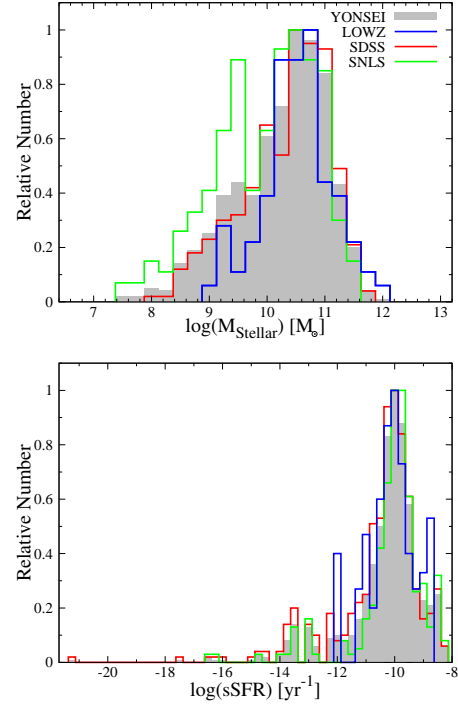


Figure 15. Same as Figure 14, but in $M_{stellar}$ (upper panel) and $sSFR$ (lower panel). We note that the LOWZ sample (blue histogram) has more fraction of high-mass ($\log(M_{stellar}) > 10.0$) hosts than that in other samples. In $sSFR$, the distributions are fairly similar each other.

Pan et al. 2014; Jones et al. 2015).

2.5.1. Kim et al. (2018) Method to Infer the Local Environments of Type Ia Supernovae

Recent studies of SN Ia host galaxy have focused on the local environments at the SN explosion site (e.g., Rigault et al. 2013, 2015, 2018; Jones et al. 2015, 2018b). However, the local environmental measurements are challenging, and so only SNe at the low-redshift range ($z < 0.1$) were available for those studies. In order to select a sample over a wider redshift range, Kim et al. (2018) introduced an empirical method to infer the local environments, only based on the global properties of host galaxies, such as $M_{stellar}$ and global $sSFR$. The main idea is that SNe Ia in locally star-forming environments can be selected when their hosts are globally star-forming and low-mass galaxies. For the SNe Ia exploding in globally passive host galaxies, all of them are also in locally passive environments, which is demonstrated by Rigault et al. (2013). We also apply this method to infer the local environments of our sample and the local sample sizes are also listed in Table 5.

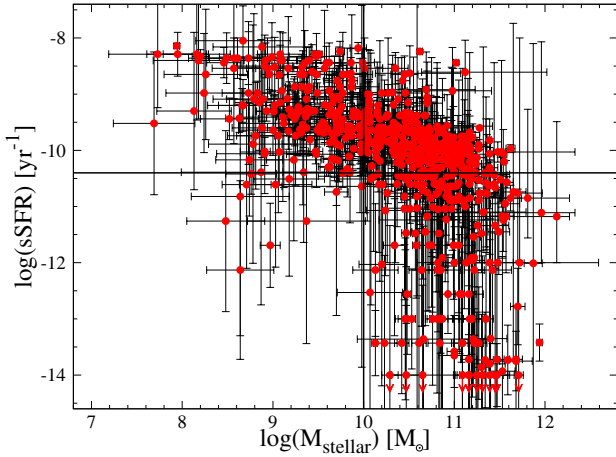


Figure 16. Distribution of M_{stellar} and $sSFR$ for the YONSEI host sample. As we expected, most of high-mass galaxies have the lower value of $sSFR$, while the low-mass galaxies universally show a strong star formation activity. The black horizontal line shows the cut criterion when we split galaxies into star-forming and passive environments at $\log(sSFR) = -10.4$. The black vertical line represents the cut criterion ($\log(M_{\text{stellar}}) = 10.0$) when we split host galaxies into high- and low-mass galaxies.

3. THE DEPENDENCE OF TYPE IA SUPERNOVA LUMINOSITIES ON THE HOST GALAXY PROPERTIES⁶

3.1. Supernova Light-Curve Fit Parameters as a Function of Host Galaxy Properties

In Figures 17 and 18, we plot the SN Ia light-curve fit parameters as a function of host global properties for SALT2 and MLCS2k2, respectively. The weighted mean of light-curve fit parameters in different host properties are summarized in Table 6.

3.1.1. Light-Curve Shape: X_1 and Δ

We start by examining the trend of SN Ia light-curve shape with host properties in the top panels of Figures 17 and 18. Overall, we recover the trend in previous works (e.g., Filippenko 1989; Hamuy et al. 1995, 1996a, 2000; Gallagher et al. 2005; Sullivan et al. 2006; Howell et al. 2009; Neill et al. 2009; Lampeitl et al. 2010; Smith et al. 2012; Childress et al. 2013; Pan et al. 2014).

First, we see the light-curve shape trend with the host galaxy morphology in the first two panels of the top panels of Figures 17 and 18. The light-curves of SNe Ia in late-type host galaxies are significantly ($>6.0\sigma$) broader and slower declining than those in early-type hosts (see also Table 6). The faintest SNe Ia are found in early-type hosts, while the most brightest SNe are found in late-type hosts. When we look at the trend with more specific morphological types of hosts (the

⁶We note that in this paper we only present the result values related to the local environmental dependence of SN Ia properties. Figures and more detailed analysis of the local environmental study can be found in Kim et al. (2018).

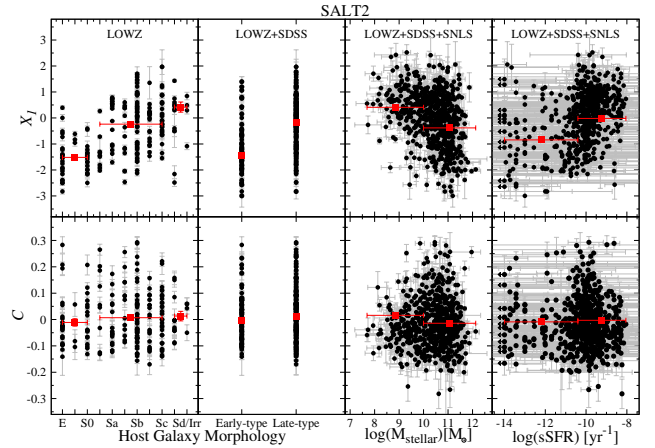


Figure 17. SALT2 light-curve fit parameters, X_1 (top panels) and C (bottom panels), as a function of host galaxy properties for the YONSEI host sample. The red squares represent the weighted means of each light-curve fit parameter in bins of host galaxy information.

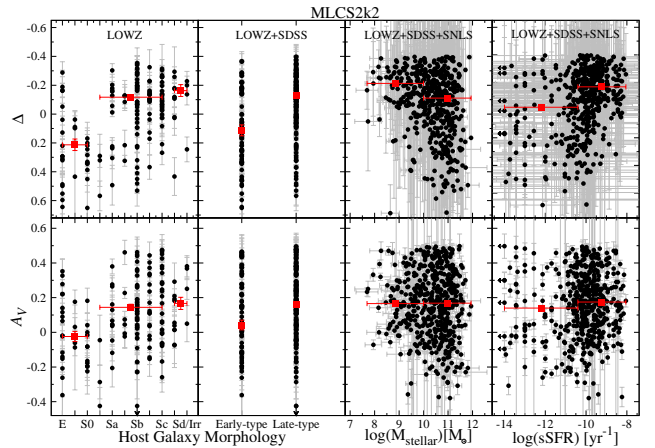


Figure 18. Same as Figure 17, but for MLCS2k2, Δ (top panels) and A_V (bottom panels).

first panel in the figures), the difference in light-curve shape parameters between SNe in E-S0 and Scd/Sd/Irr hosts is $\sim 55\%$ increased compared to when splitting the sample into early- and late-types. Considering the stellar population age difference between those morphological types, this result indirectly shows that there could be a different population age in the SN progenitors.

The light-curve shape parameters as a function of host M_{stellar} and global $sSFR$ can be found in the third and fourth panels of the top panels of Figures 17 and 18. The figures show that broader and slower declining SNe Ia are more likely to be found in low-mass and globally star-forming hosts at a $>6.5\sigma$ confidence level (see also Table 6). Note that, in low-mass and high $sSFR$ hosts, narrower and faster declining SNe are rarer, while SNe in high-mass and low $sSFR$ have a much wider light-curve shape range. We also see evidence that the light-curve shape parameter is a continuous variable of

Table 6
The Weighted Mean of Light-Curve Fit Parameters in Different Host Properties

Host Property	Group	SALT2					MLCS2k2				
		N_{SN}	$X_{1,WM}$	Error	C_{WM}	Error	N_{SN}	Δ_{WM}	Error	$A_{V,WM}$	Error
Morphology	E-S0	44	-1.515	0.079	-0.011	0.014	32	0.213	0.040	-0.024	0.029
	S0a-Sc	134	-0.238	0.083	0.007	0.009	106	-0.117	0.019	0.144	0.018
	Scd/Sd/Irr	16	0.420	0.194	0.013	0.018	14	-0.163	0.041	0.167	0.035
Diff.	(Scd/Sd/Irr - E-S0)		1.935	0.209	0.024	0.023		0.376	0.057	0.191	0.045
Morphology	Early-type	68	-1.426	0.079	-0.003	0.011	51	0.113	0.038	0.042	0.028
	Late-type	181	-0.180	0.070	0.011	0.007	146	-0.130	0.015	0.159	0.015
	Diff.		1.246	0.106	0.014	0.013		0.243	0.041	0.117	0.032
Mass	High-mass	469	-0.383	0.046	-0.014	0.004	369	-0.111	0.011	0.168	0.009
	Low-mass	188	0.410	0.048	0.016	0.007	143	-0.213	0.011	0.166	0.013
	Diff.		0.793	0.066	0.030	0.008		0.102	0.016	0.002	0.016
sSFR	Globally Passive	196	-0.844	0.070	-0.009	0.007	155	-0.021	0.020	0.140	0.015
	Globally Star-Forming	461	-0.016	0.041	-0.003	0.004	357	-0.169	0.011	0.175	0.009
	Diff.		0.828	0.081	0.006	0.008		0.148	0.023	0.035	0.017
sSFR	Locally Passive	196	-0.844	0.070	-0.009	0.007	155	-0.021	0.020	0.140	0.015
	Locally Star-Forming	177	0.455	0.046	0.017	0.007	134	-0.219	0.011	0.167	0.013
	Diff.		1.299	0.084	0.026	0.010		0.198	0.023	0.027	0.020

$M_{stellar}$ and global $sSFR$, as pointed out by Sullivan et al. (2010).

3.1.2. Supernova Color and Host Extinction: C and A_V

Lower panels of Figures 17 and 18 show the trend of the SN Ia color for SALT2 and the host extinction for MLCS2k2 with host properties, respectively. The situation in interpreting SN Ia color is very complicated, as C is a single parameter that captured both SN intrinsic color and host reddening by dust. Even though several studies discussed on this issue (e.g., Hicken et al. 2009b; Neill et al. 2009; Sullivan et al. 2010; Childress et al. 2013; Pan et al. 2014), there is no conclusive result yet. For the MLCS2k2 A_V , this is the first time in SN host studies to investigate the trend with host $M_{stellar}$ and $sSFR$.

The SN color trend with host properties can be found in the lower panels of Figure 17. At first, we would expect that SNe Ia in late-type and globally star-forming host galaxies are redder, because these galaxies are thought to contain more dust than early-type and globally passive galaxies in general. However, no strong trends are found with host morphological types and global $sSFR$. On the other hand, we find a mild trend with the host stellar mass. SNe Ia in high-mass hosts show slightly bluer than those in low-mass hosts: the difference in the weighted mean of C is 0.030 ± 0.008 (3.8σ , Table 6). We note that the reddest SNe Ia (e.g., $C \geq 0.2$) prefer high-mass and globally star-forming hosts.

In the lower panels of Figure 18, we plot the dust extinction value for host galaxies estimated from MLCS2k2 as a function of host properties. As expected, we find that late-type and globally star-forming host galaxies show 0.117 ± 0.032 mag (3.7σ) and 0.035 ± 0.017 mag (2.1σ) higher extinction value than early-type and globally passive hosts, respectively (see Table 6). The difference is the largest (0.191 ± 0.045 mag, 4.2σ) when

we split the hosts into more specific morphological types. In contrary to SALT2 C , there is no trend with $M_{stellar}$.

3.2. Luminosity Dependence of Type Ia Supernovae on the Properties of Host Galaxies

As we observed in the above section, the trends between light-curve fit parameters and host properties require a correction for the light-curve shape and color or extinction. If the correction perfectly works, we would not be able to observe the dependence of “corrected” luminosity of SNe Ia on the properties of host galaxies. In order to investigate this environmental effect, we plot the corrected luminosity of SNe Ia as a function of host global properties in Figures 19 through 25. The weighted mean and rms scatter of HRs with host properties for our sample are listed in Table 7.

For this investigation, as we have briefly introduced in Section 2.4.1, we use the definition of the Hubble residual (HR) for the corrected luminosity of SNe Ia. HR is defined as $HR \equiv \mu_{SN} - \mu_{model}(z)$, so that a negative residual means that the distance determined from the SN is less than the distance derived from the host galaxy redshift, together with the cosmological model. Therefore, in general, we interpret that the brighter SNe, after light-curve corrections, have negative HRs, and vice versa for the fainter SNe. In the calculation of the weighted mean of HRs in each host group, the error of the weighted mean is corrected to ensure a $\chi_{red}^2 = 1$. We have also applied Chauvenet’s criterion to reject outliers during this procedure. For our analysis, this criterion corresponds to 2.9σ for SALT2 and 2.8σ for MLCS2k2, on average.

3.2.1. Host Stellar Mass

We start with a well-established correlation between SN HRs and host $M_{stellar}$. In Figure 19, the dependence of SN Ia luminosity on the host $M_{stellar}$ is shown for

Table 7
The Weighted Mean and rms Scatter of Hubble Residuals in Different Host Properties

Host Property	Group	SALT2					MLCS2k2				
		N_{SN}	HR _{WM} (mag)	Error (mag)	rms (mag)	Error (mag)	N_{SN}	HR _{WM} (mag)	Error (mag)	rms (mag)	Error (mag)
Mass	High-mass	464	-0.022	0.008	0.172	0.006	366	-0.023	0.009	0.166	0.006
	Low-mass	184	0.035	0.012	0.164	0.009	138	0.042	0.012	0.140	0.008
Diff.			0.057	0.014				0.065	0.015		
sSFR	Globally Passive	194	-0.043	0.013	0.180	0.009	152	-0.034	0.013	0.162	0.009
	Globally Star-Forming	455	0.006	0.008	0.167	0.006	354	-0.001	0.009	0.163	0.006
Diff.			0.049	0.015				0.033	0.016		
sSFR	Locally Passive	194	-0.043	0.013	0.180	0.009	152	-0.034	0.013	0.162	0.009
	Locally Star-Forming	174	0.038	0.013	0.172	0.009	129	0.038	0.012	0.138	0.009
Diff.			0.081	0.018				0.072	0.018		
Morphology	E-S0	44	0.036	0.036	0.220	0.022	32	0.038	0.036	0.187	0.024
	S0a-Sc	131	0.001	0.018	0.191	0.012	103	-0.014	0.019	0.176	0.012
	Scd/Sd/Irr	16	0.018	0.038	0.119	0.013	14	0.073	0.028	0.049	0.010
Diff.	(Scd/Sd/Irr - E-S0)		0.018	0.052				0.035	0.046		
Morphology	Early-type	66	-0.012	0.023	0.178	0.016	50	-0.019	0.024	0.164	0.017
	Late-type	177	-0.009	0.014	0.173	0.009	143	0.001	0.015	0.162	0.010
Diff.			0.003	0.027				0.020	0.028		

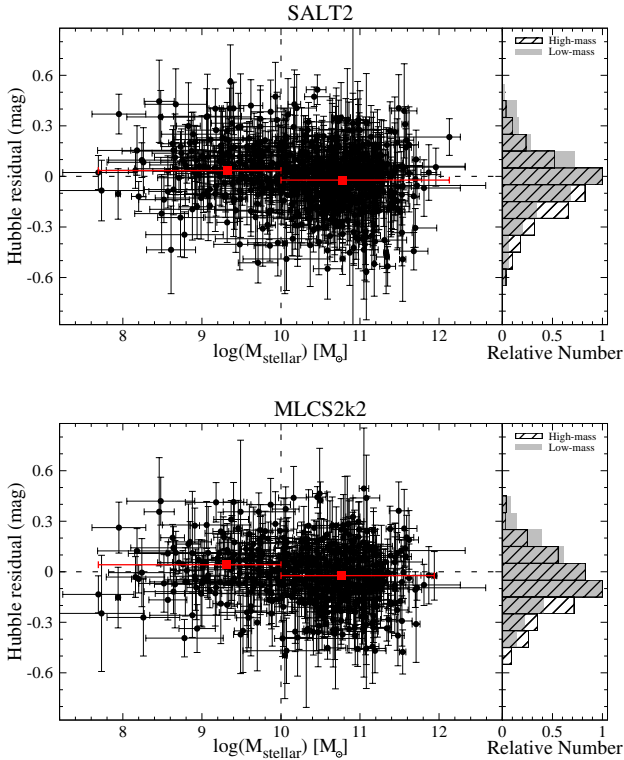


Figure 19. HRs for SALT2 (upper panel) and MLCS2k2 (lower panel) versus host $M_{stellar}$. We find that SNe Ia in the low-mass hosts are ~ 0.06 mag fainter than those in the high-mass hosts. The red squares represent the weighted means of HRs in bins of host $M_{stellar}$. The vertical dotted line ($\log(M_{stellar}) = 10.0$) indicates the limit distinguishing between high-mass and low-mass host galaxies. The histogram on the right panel shows the HR distribution of SNe Ia in high-mass and low-mass hosts.

SALT2 (upper panel) and MLCS2k2 (lower panel). We find that SNe Ia in the low-mass hosts are fainter than those in the high-mass hosts: the difference in the weighted mean of HRs is 0.057 ± 0.014 mag (4.1σ) for SALT2 and 0.065 ± 0.015 mag (4.3σ) for MLCS2k2 (see Table 7). Our findings are quantitatively and qualitatively well consistent with the previous studies (e.g., Kelly et al. 2010; Lampeitl et al. 2010; Sullivan et al. 2010).

We also investigate the difference in HRs for LOWZ (low-redshift), SDSS (intermediate-redshift), and SNLS (high-redshift) samples separately. In Figures 20 and 21, the dependence of SN Ia luminosity on the host $M_{stellar}$ split by SN data is shown for SALT2 and MLCS2k2, respectively. Each subsample in the different redshift range follows the trend as we found with the YONSEI sample, and their HR differences are consistent within the $\sim 1\sigma$ level (see Table 8). This would indicate that the SN Ia luminosity dependence on the host $M_{stellar}$ is the global phenomenon over the whole redshift range. We note that because the LOWZ sample was discovered in host-targeted surveys which prefer more luminous and massive galaxies, as we pointed out in Section 2.5, there is a large imbalance between the fraction of low-mass and high-mass host galaxies (e.g., 15:85, compared to 31:69 for other samples on average). This may affect the trend in the LOWZ sample.

Finally, we compare the rms scatters for SNe Ia in the high-mass and those in the low-mass samples. SNe in low-mass hosts show $\sim 5\%$ and $\sim 16\%$ smaller rms scatter than those in high-mass hosts for SALT2 and MLCS2k2, respectively (see Table 7). This result appears to be that SNe Ia in the low-mass hosts are better standard candles than those in the high-mass hosts.

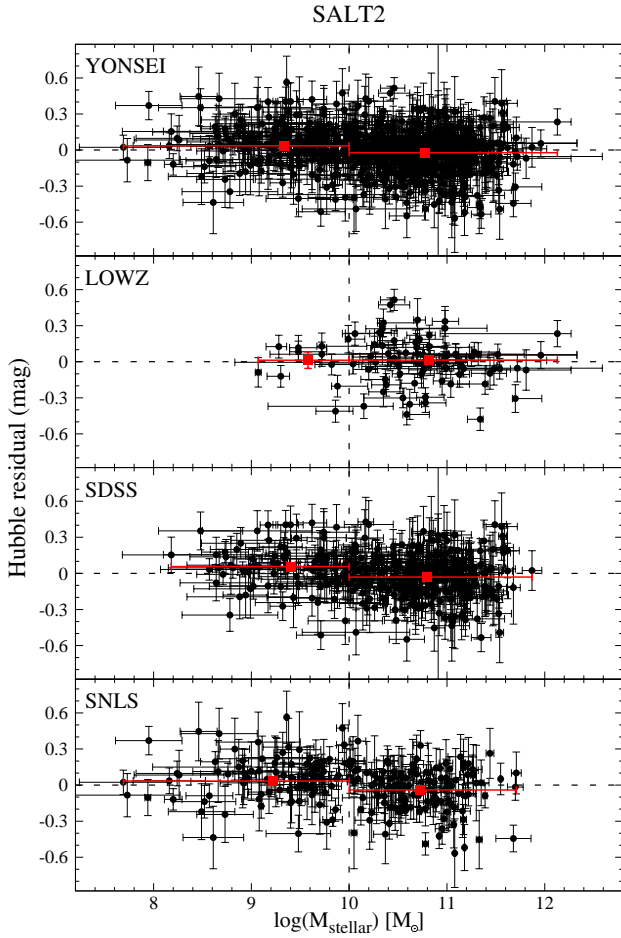


Figure 20. SALT2 HRs versus M_{stellar} of host galaxies observed by surveys. Each subsample in the different redshift range follows the trend as we found with the YONSEI sample.

3.2.2. Host Global Specific Star Formation Rate

We plot the dependence of SN Ia luminosity on the host global $sSFR$ in Figure 22. We find that SNe Ia in the globally star-forming hosts are 0.049 ± 0.015 mag (3.3σ) and 0.033 ± 0.016 mag (2.1σ) fainter than those in the globally passive hosts for SALT2 and MLCS2k2, respectively (see Table 7). Our result is qualitatively consistent with previous results, but the HR differences are reduced (e.g., ~ 0.100 mag, see Lampeitl et al. 2010; Sullivan et al. 2010; D’Andrea et al. 2011). We note that the weighted mean of HR for SNe Ia in globally star-forming hosts interestingly shows ~ 0.0 mag, which implies that those SNe can be a good anchor for the Hubble–Lemaître diagram.

In Figures 23 and 24, the SN Ia luminosity trends with host global $sSFR$ split by SN data are shown for SALT2 and MLCS2k2, respectively. The trends in each subsample in the different redshift range agree well with the trend observed in the YONSEI sample, even though at slightly lower significance (see Table 8). As the mean $sSFR$ is known to increase with redshift (e.g., Madau & Dickinson 2014; Driver et al. 2018), the fraction of glob-

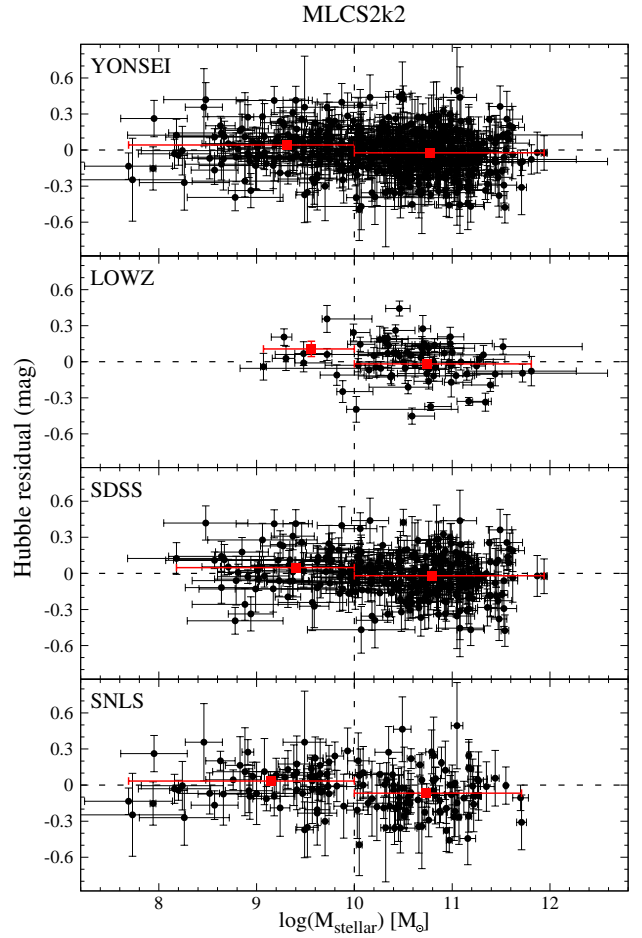


Figure 21. Same as Figure 20, but for MLCS2k2 HRs.

ally star-forming hosts in our sample is also increased by $\sim 10\%$ with redshift. In addition, the overall SN Ia occurrence rate of globally star-forming hosts in the YONSEI sample is ~ 2.3 times larger than that of globally passive hosts, and this is qualitatively consistent with the results of Sullivan et al. (2006) and Smith et al. (2012).

The rms scatter of SNe Ia in globally star-forming hosts shows a $\sim 7\%$ less scatter than those in globally passive hosts for SALT2. However, we see no difference in the rms scatter for the MLCS2k2 global $sSFR$ sample. Previous studies also reached different conclusions for each author. For example, Kelly et al. (2015), Uddin et al. (2017), and Kim et al. (2018) supported that SNe Ia in the star-forming sample show a less scatter, while Lampeitl et al. (2010), Sullivan et al. (2010), and Jones et al. (2015) found the opposite result.

3.2.3. Host Morphology

Figure 25 shows the dependence of SN Ia luminosity on the host galaxy morphology for SALT2 (upper panel) and MLCS2k2 (lower panel). We observe no conclusive trends for our LOWZ and intermediate-redshift SDSS samples. More quantitatively, the HR difference is 0.011 ± 0.029 mag and 0.028 ± 0.027 mag on average

Table 8
Summary of Hubble Residual Differences in Each Data Set

SN Data	SALT2					
	Mass			sSFR		
	N_{SN}	$N_{Low} : N_{High}$	HR Diff. (mag)	N_{SN}	$N_{Pas} : N_{SF}$	HR Diff. (mag)
YONSEI	648	184:464	0.057 ± 0.014 (4.1σ)	649	194:455	0.049 ± 0.015 (3.3σ)
LOWZ	88	12:76	0.002 ± 0.072 (0.0σ)	86	28:59	0.054 ± 0.044 (1.2σ)
SDSS	350	87:263	0.088 ± 0.018 (4.9σ)	350	122:228	0.040 ± 0.019 (2.1σ)
SNLS	207	85:122	0.074 ± 0.023 (3.2σ)	207	45:162	0.069 ± 0.031 (2.2σ)

SN Data	MLCS2k2					
	Mass			sSFR		
	N_{SN}	$N_{Low} : N_{High}$	HR Diff. (mag)	N_{SN}	$N_{Pas} : N_{SF}$	HR Diff. (mag)
YONSEI	504	138:366	0.065 ± 0.015 (4.3σ)	506	152:354	0.033 ± 0.016 (2.1σ)
LOWZ	71	11:60	0.124 ± 0.068 (1.8σ)	72	18:54	0.013 ± 0.042 (0.3σ)
SDSS	288	69:219	0.066 ± 0.019 (3.5σ)	287	99:188	0.042 ± 0.019 (2.2σ)
SNLS	140	57:83	0.102 ± 0.025 (4.1σ)	141	36:105	0.061 ± 0.037 (1.6σ)

for SALT2 and MLCS2k2, respectively (see Table 7). The results show a greatly reduced difference in HRs compared to the previous results, which found the HR difference of 0.144 ± 0.070 mag for the low-redshift sample ($z < 0.1$; Hicken et al. 2009b) and 0.180 ± 0.090 mag for the high-redshift sample ($z > 0.9$; Suzuki et al. 2012).

We also find that SNe Ia in Scd/Sd/Irr hosts have the lowest rms scatter (~ 0.084 mag, see Table 7), which is consistent with the result of Hicken et al. (2009b). These SNe show a 46% and 74% smaller rms scatter than those in E-S0 hosts for SALT2 and MLCS2k2, respectively. This may imply that SNe Ia exploded in Scd/Sd/Irr hosts would provide more robust results in estimating cosmological parameters.

3.2.4. Comparison with Previous Studies

In this section, we summarize our findings of the difference in SN Ia HRs in different host galaxy properties and compare them with the results reported in previous studies. We present a summary of our findings and previous results in Table 9 and Figure 26. We note that we compare our results only with those which used corrections for both the light-curve shape and SN color or host extinction (e.g, after 2007, when Guy et al. 2007 and Jha et al. 2007 released SALT2 and MLCS2k2 fitters, respectively).

We first compare our result with previous studies with respect to host $M_{stellar}$. As shown in the table, there are many studies with a variety of samples over a large redshift range. They found that SNe Ia in high-mass hosts appear brighter than those in low-mass hosts, after light-curve corrections with several light-curve fitters. The size of HR difference is 0.08 mag on average and the transition mass is around $10^{10} M_{\odot}$. Our result indeed is fully consistent with previous studies within the $\sim 1\sigma$ level.

Several points in the table for the mass comparison are worth noting here. The first is that some of the recent studies tried to include photometrically classified SNe Ia in their sample (e.g., Campbell et al. 2016; Ud-

din et al. 2017; Jones et al. 2018a). With this inclusion, their sample size is ~ 2 times larger than other studies. The error of the HRs, however, is not small as much as expected from the sample size, because of the contamination from other types of SNe. The second one of note regards the light-curve fitting method for the results of Jones et al. (2018a) and Scolnic et al. (2018). They employed the same equation for the SALT2 SN distance modulus as we used (see Equation 1), but they included two extra terms: Δ_M for the host mass dependence correction and Δ_B for the simulated selection bias correction (see Equation 3). Interestingly, even though they considered the HR difference among different host masses prior to estimating the distance modulus of SNe, the dependence of SN Ia luminosity on the host mass is still observed at $\sim 5.2\sigma$ level. The last note is that Scolnic et al. (2014) found no trend between HRs and host stellar mass. However, the interesting point is that with a ~ 10 times larger sample which includes Scolnic et al. (2014) data, the trend is recovered in Scolnic et al. (2018).

We now turn to the results of host global $sSFR$. Our result is consistent with previous studies in the sense that SNe Ia in passive hosts are brighter than those in star-forming hosts. The size of HR difference is 0.06 mag on average. However, the size of difference is smaller and shows statistically less significant than the result split by host $M_{stellar}$.

Assuming that host $M_{stellar}$ and $sSFR$ are closely related to the galaxy morphology, we expect from above that brighter SNe Ia would be exploded in the early-type host galaxies. However, we find no HR difference between SNe Ia in early-type hosts and those in late-type hosts, while previous studies found at $\sim 2\sigma$ level. This may be because our LOWZ sample, which is dominant in the host morphology study ($\sim 80\%$), is drawn from a host-targeted survey, as pointed out in Section 2.5. It leads to that most of the hosts in the LOWZ sample are in the high-mass region (see the second panels of Figures 20 and 21), thus there would be no HR difference between SNe in early-type hosts and

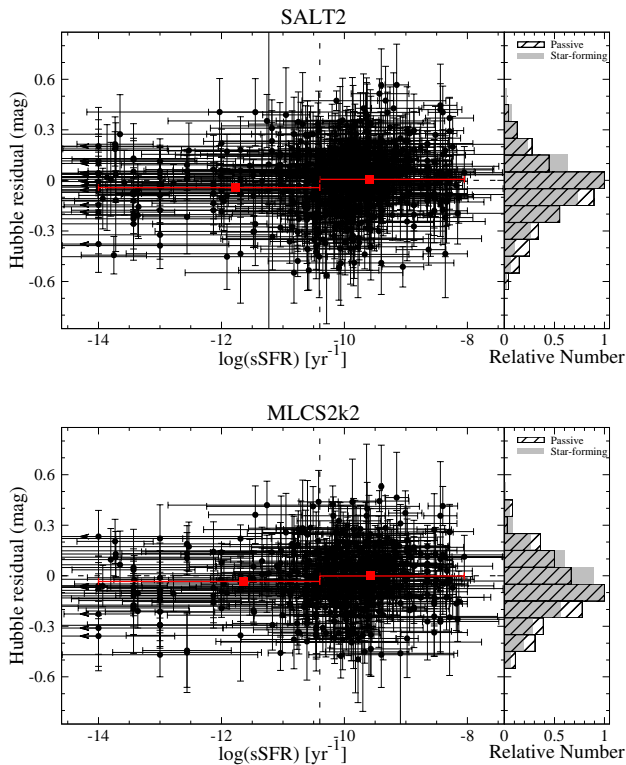


Figure 22. Same as Figure 19, but for global $sSFR$ of host galaxies. We find that SNe Ia in the globally star-forming hosts are ~ 0.04 mag fainter than those in the globally passive hosts. The vertical dotted line ($\log(sSFR) = -10.4$) indicates the limit distinguishing between passive and star-forming host galaxies for our sample. The histogram on the right panel shows the HR distribution of SNe Ia in passive and star-forming hosts.

those in late-type hosts.

Finally, we look at the trends with local environments of SNe Ia. Our finding which includes a sample at high-redshift range shows a good agreement with previous results. They concluded that SNe Ia occurring locally passive and redder in local $U - V$ color are brighter than those in locally star-forming and bluer color environments, except the results of Jones et al. (2015)⁷. The size of HR difference is ~ 0.1 mag, which is a larger difference than when using host global properties. As the local environment is more directly linked to the SN progenitor, the results strongly suggest that there are different populations in SN Ia progenitor.

From this comparison, we conclude that our results are consistent with the results reported by many previous studies. However, our findings are an independent confirmation based on the spectroscopically confirmed SNe Ia from a combined sample of LOWZ, SDSS, and SNLS data, together with two different light-curve fitters.

⁷This is because of the effect of the redshift cut they applied for their sample. Kim et al. (2018) recovered the Jones et al. (2015) and Rigault et al. (2015) results, which show an apparent discrepancy, by applying the same redshift cut used by each of them.

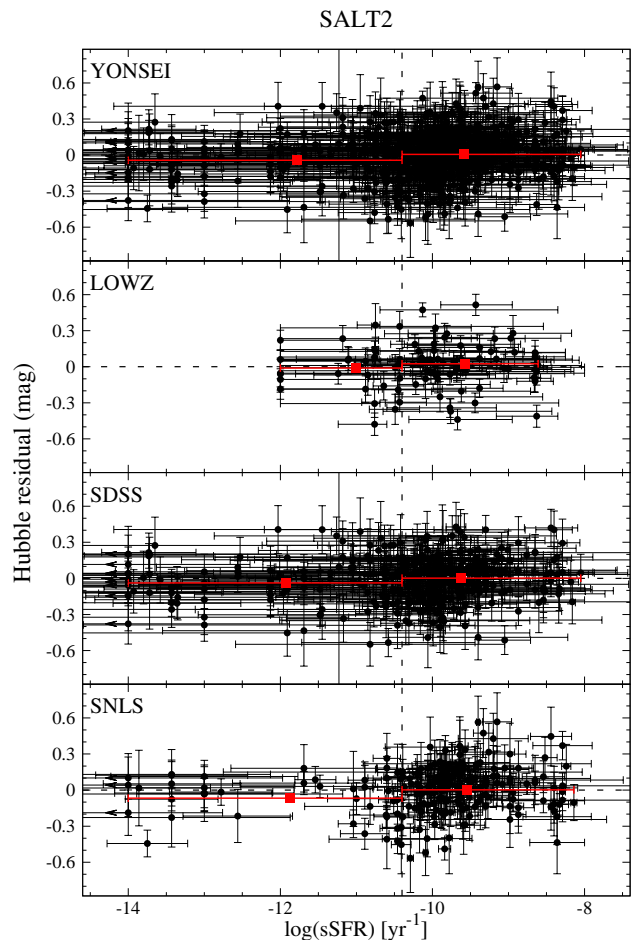


Figure 23. SALT2 HRs versus global $sSFR$ of host galaxies observed by surveys. The trends in each subsample in the different redshift range agree well with the trend observed in the YONSEI sample.

4. ESTIMATING COSMOLOGICAL PARAMETERS FROM SNE IA IN DIFFERENT ENVIRONMENTS

We observed in the previous section that the luminosity of SNe Ia varies with their host properties. This would imply that using a whole sample of SNe Ia together without considering host environments can cause a bias in estimating cosmological parameters; for example, a $\sim 10\%$ shift in w and a 3.3% correction for H_0 (Lampeitl et al. 2010; Sullivan et al. 2010, 2011; Rigault et al. 2013, 2015; Campbell et al. 2016; Uddin et al. 2017). In order to investigate this bias in the YONSEI Cosmology sample, here we split the SN Ia sample according to the host environments as following the previous section (e.g., see Table 7), and then estimate cosmological parameters separately.

We use the same JLA likelihood code as we described in Section 2.4.1 to estimate the best-fit cosmological parameters from SALT2 SNe Ia alone. For our baseline cosmology, we assume the flat Λ CDM model. One difference from the Section 2.4.1 is that here we simultaneously calculate σ_{int} , instead of setting $\sigma_{int} = 0$. As σ_{int} is the uncertainty that makes a χ^2_{red} equals

Table 9
Comparison of Hubble Residual Differences between Previous Studies

Study	SN Data	N_{SN}	Redshift Range	HR Diff. (mag)	LC Fitter
Mass					
This Work	YONSEI	648	$0.01 < z < 0.85$	0.057 ± 0.014 (4.1σ)	SALT2
This Work	YONSEI	504	$0.01 < z < 0.85$	0.065 ± 0.015 (4.3σ)	MLCS2k2 ($R_V = 2.2$)
Kelly et al. (2010)	CfA	62	$0.015 < z < 0.08$	0.094 ± 0.045 (2.1σ)	SALT2
Kelly et al. (2010)	CfA	60	$0.015 < z < 0.08$	0.083 ± 0.046 (1.8σ)	MLCS2k2
Lampeitl et al. (2010)	SDSS	162	$0.05 < z < 0.21$	0.100 ± 0.025 (4.0σ)	SALT2
Sullivan et al. (2010)	SNLS	195	$0.01 < z < 0.85$	0.080 ± 0.020 (4.0σ)	SALT2+SiFTO
Gupta et al. (2011)	SDSS	206	$0.01 < z < 0.42$	0.096 ± 0.028 (3.4σ)	SALT2
Childress et al. (2013)	SNf	115	$0.03 < z < 0.08$	0.085 ± 0.028 (3.0σ)	SALT2
Rigault et al. (2013)	SNf	82	$0.03 < z < 0.08$	0.098 ± 0.031 (3.2σ)	SALT2
Betoule et al. (2014)	JLA	740	$0.01 < z < 1.4$	0.061 ± 0.012 (5.1σ)	SALT2
Pan et al. (2014)	PTF	50	$0.01 < z < 0.09$	0.085 ± 0.047 (1.8σ)	SiFTO
Scolnic et al. (2014)	PS	110	$0.03 < z < 0.65$	0.019 ± 0.025 (0.8σ)	SALT2
Campbell et al. (2016)	SDSS	581 ^a	$0.05 < z < 0.55$	0.091 ± 0.045 (2.0σ)	SALT2
Wolf et al. (2016)	SDSS	144	$0.05 < z < 0.3$	0.082 ± 0.030 (2.7σ)	SALT2
Uddin et al. (2017)	CfA+CSP+SDSS+SNLS	1338 ^b	$0.01 < z < 1.1$	0.050 ± 0.009 (5.6σ)	SALT2
Jones et al. (2018a)	CfA+CSP+PS	1369 ^c	$0.01 < z < 0.7$	0.092 ± 0.021 (4.4σ)	SALT2 with Δ_M and Δ_B^d
Jones et al. (2018b)	Pantheon+Foundation	216	$0.01 < z < 0.1$	0.049 ± 0.018 (2.7σ)	SALT2 with Δ_B^d
Rigault et al. (2018)	SNf	141	$0.02 < z < 0.08$	0.119 ± 0.026 (4.6σ)	SALT2
Roman et al. (2018)	CfA+CSP+SDSS+SNLS	666	$0.01 < z < 0.8$	0.070 ± 0.013 (5.4σ)	SALT2
Scolnic et al. (2018)	Pantheon	1023	$0.01 < z < 2.3$	0.053 ± 0.009 (5.9σ)	SALT2 with Δ_M and Δ_B^d
Global Specific Star Formation Rate					
This Work	YONSEI	649	$0.01 < z < 0.85$	0.049 ± 0.015 (3.3σ)	SALT2
This Work	YONSEI	506	$0.01 < z < 0.85$	0.033 ± 0.016 (2.1σ)	MLCS2k2 ($R_V = 2.2$)
Lampeitl et al. (2010)	SDSS	162	$0.05 < z < 0.21$	0.100 ± 0.040 (2.5σ)	SALT2
Sullivan et al. (2010)	SNLS	195	$0.01 < z < 0.85$	0.080 ± 0.031 (2.6σ)	SALT2+SiFTO
D'Andrea et al. (2011)	SDSS	55	$z < 0.15$	0.100 ± 0.033 (3.0σ)	SALT2
Childress et al. (2013)	SNf	115	$0.03 < z < 0.08$	0.050 ± 0.029 (1.7σ)	SALT2
Pan et al. (2014)	PTF	48	$0.01 < z < 0.09$	0.070 ± 0.041 (1.7σ)	SiFTO
Wolf et al. (2016)	SDSS	144	$0.05 < z < 0.3$	0.013 ± 0.031 (0.5σ)	SALT2
Uddin et al. (2017)	CfA+CSP+SDSS+SNLS	1338 ^c	$0.01 < z < 1.1$	0.030 ± 0.014 (2.1σ)	SALT2
Morphology					
This Work	YONSEI	243	$0.01 < z < 0.2$	0.003 ± 0.027 (0.1σ)	SALT2
This Work	YONSEI	193	$0.01 < z < 0.2$	0.020 ± 0.028 (0.7σ)	MLCS2k2 ($R_V = 2.2$)
Hicken et al. (2009b)	CfA	97	$0.01 < z < 0.1$	0.144 ± 0.070 (2.1σ)	SALT2+MLCS2k2
Suzuki et al. (2012)	Union2.1	28	$0.9 < z < 1.5$	0.180 ± 0.090 (2.0σ)	SALT2
Local Environments					
This Work	YONSEI	281	$0.01 < z < 0.85$	0.072 ± 0.018 (4.0σ)	MLCS2k2 ($R_V = 2.2$)
Rigault et al. (2013)	SNf	82	$0.03 < z < 0.08$	0.094 ± 0.031 (4.5σ)	SALT2
Jones et al. (2015)	CfA+CSP+CT+SDSS+SNLS+PS1	179	$0.01 < z < 0.1$	0.000 ± 0.018 (0.0σ)	SALT2
Jones et al. (2015)	CfA+CSP+CT+SDSS+SNLS+PS1	156	$0.01 < z < 0.1$	0.029 ± 0.027 (1.1σ)	MLCS2k2 ($R_V = 2.5$)
Rigault et al. (2015)	CfA	77	$0.023 < z < 0.1$	0.094 ± 0.037 (2.5σ)	SALT2
Rigault et al. (2015)	CfA	81	$0.023 < z < 0.1$	0.155 ± 0.041 (3.8σ)	MLCS2k2 ($R_V = 2.5$)
Jones et al. (2018b)	Pantheon+Foundation	195	$0.01 < z < 0.1$	0.040 ± 0.020 (2.0σ)	SALT2 with Δ_B^d
Kim et al. (2018)	YONSEI	368	$0.01 < z < 0.85$	0.081 ± 0.018 (4.5σ)	SALT2
Rigault et al. (2018)	SNf	141	$0.02 < z < 0.08$	0.163 ± 0.029 (5.6σ)	SALT2
Roman et al. (2018)	CfA+CSP+SDSS+SNLS	666	$0.01 < z < 0.8$	0.091 ± 0.013 (7.0σ)	SALT2

a. 581 photometrically classified SNe Ia.

b. 755 photometrically classified SNe Ia are included in their SDSS and SNLS samples.

c. 1035 photometrically classified SNe Ia are included in their PS sample.

d. Δ_M is a distance correction based on the host mass and Δ_B is another distance correction based on the predicted selection bias estimated from SN survey simulations.

Table 10
Best-Fit Flat Λ CDM Parameters Estimated from SNe Ia in Different Host Environments

Group	SNe	Ω_M	α	β	M_B	σ_{int}	$\chi^2/D.O.F.$
High-Mass	464	$0.32^{+0.12}_{-0.08}$	$0.15^{+0.01}_{-0.02}$	3.26 ± 0.20	$-19.07^{+0.03}_{-0.02}$	0.112	458.23/460
Low-Mass	184	$0.29^{+0.09}_{-0.06}$	0.15 ± 0.03	$3.28^{+0.36}_{-0.34}$	$-19.03^{+0.05}_{-0.04}$	0.098	179.37/180
Globally Passive	194	$0.33^{+0.09}_{-0.10}$	$0.18^{+0.03}_{-0.02}$	$2.96^{+0.31}_{-0.29}$	$-19.12^{+0.04}_{-0.05}$	0.104	190.62/190
Globally Star-Forming	455	0.30 ± 0.05	$0.13^{+0.02}_{-0.01}$	$3.28^{+0.19}_{-0.20}$	$-19.06^{+0.02}_{-0.03}$	0.105	450.08/451
Locally Passive	194	$0.33^{+0.09}_{-0.10}$	$0.18^{+0.03}_{-0.02}$	$2.96^{+0.31}_{-0.29}$	$-19.12^{+0.04}_{-0.05}$	0.104	190.62/190
Locally Star-Forming	174	0.31 ± 0.09	$0.14^{+0.04}_{-0.03}$	$3.40^{+0.40}_{-0.37}$	-19.02 ± 0.05	0.111	170.58/170
YONSEI Cosmology	1049	$0.32^{+0.03}_{-0.04}$	$0.14^{+0.01}_{-0.00}$	$3.07^{+0.14}_{-0.15}$	$-19.06^{+0.01}_{-0.02}$	0.131	1038.15/1045

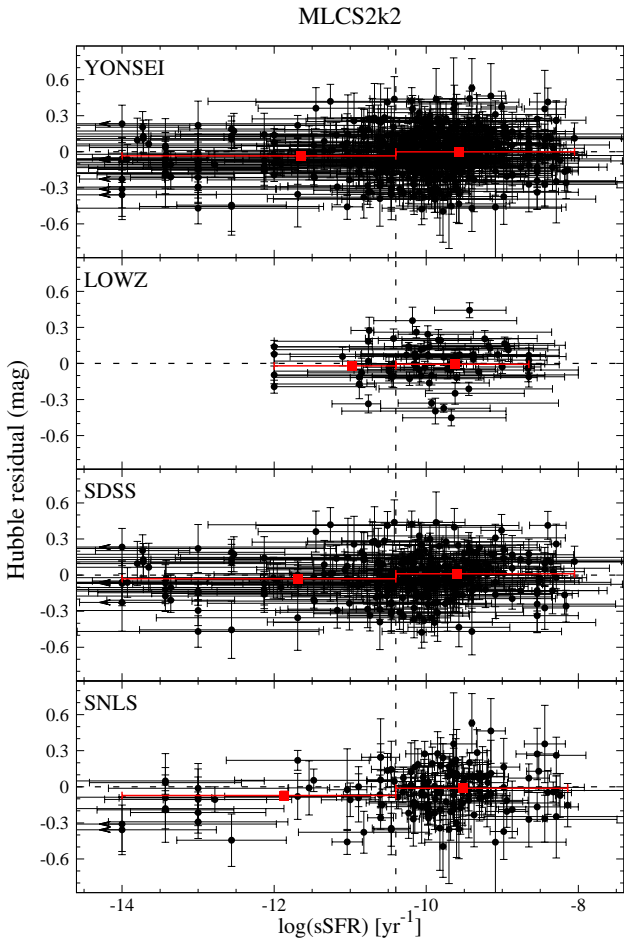


Figure 24. Same as Figure 23, but for MLCS2k2 HRs.

unity, this uncertainty is required when we determine the ‘best-fit’ cosmological parameters. The best-fit parameters estimated from the YONSEI Cosmology sample in different environments are listed in Table 10.

The table shows that shifts in Ω_M and α are negligible, as pointed out by Sullivan et al. (2011) and Uddin et al. (2017). However, in β , we can see the significant shift, except when splitting the sample based on host $M_{stellar}$. The value of β in passive environments is lower than that in star-forming environments. This trend is also observed in Lampeitl et al. (2010) with the SDSS sample and Sullivan et al. (2010) with the SNLS sample.

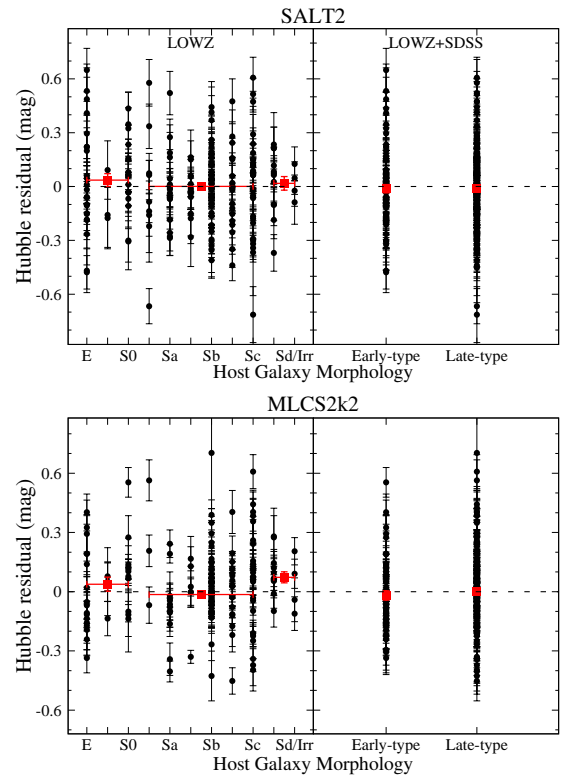


Figure 25. Same as Figure 19, but for the host galaxy morphology. We observe no conclusive trend.

In terms of σ_{int} (Table 10) and rms scatter of HRs (Table 7), SNe Ia in low-mass and star-forming environments provide more robust results when estimating cosmological parameters. For example, SNe in locally star-forming environments have a $\sim 18\%$ smaller rms scatter, and also require a $\sim 15\%$ smaller intrinsic scatter than those in the full YONSEI Cosmology sample. From this, we can consider that SNe Ia in low-mass and star-forming environments would have similar progenitor ages that represent the most homogeneous sample (see also Childress et al. 2014; Kelly et al. 2015; Kim et al. 2018).

From the results described in this section, we conclude that cosmological parameters seem to be biased when we do not consider the SN Ia environments. As more SNe Ia surveys are coming with a much larger sample than ever, it would be expected that we start

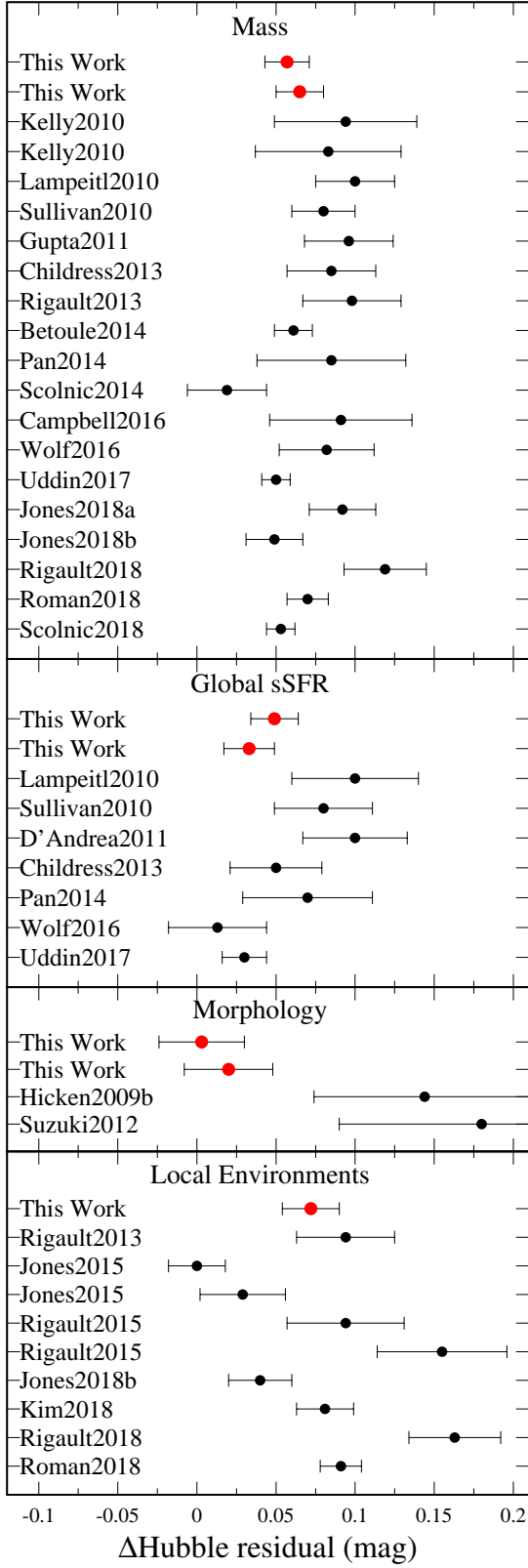


Figure 26. Comparison of HR differences between previous studies. We find that our results are consistent with the results reported by many previous studies. See Table 9 for more information about each study.

to see an obvious difference in cosmological parameters estimated from SNe Ia (Uddin et al. 2017). This means that we may need a host-related-correction (see e.g., Sullivan et al. 2011; Suzuki et al. 2012; Scolnic et al. 2018). However, investigating the origin of the environmental dependence of SN Ia luminosity should be preceded, which leads us to a more accurate cosmology.

5. DISCUSSION

The purpose of this paper is to investigate the dependence of SNe Ia luminosity on global and local properties of host galaxies, explore the origin of the dependence, and predict the impact of the luminosity dependence on the SN cosmology. For this, we have constructed an independent SN Ia catalog, which has 1231 spectroscopically confirmed SNe Ia and 674 host galaxy data over the redshift range of $0.01 < z < 1.37$ and includes two independent light-curve fitters of SALT2 and MLCS2k2. From this catalog, we find that SNe Ia in low-mass and star-forming environments are 0.062 ± 0.009 mag and 0.057 ± 0.010 mag fainter than those in high-mass and passive environments, after “empirical” light-curve corrections with SALT2 and MLCS2k2, respectively (see Table 7 for our main results). When only local environments of SNe Ia are considered, the luminosity difference increases to 0.081 ± 0.018 mag for SALT2 and 0.072 ± 0.018 mag for MLCS2k2. Our finding is consistent with previous studies (see Table 9). However, our result is an independent confirmation based on a combined sample of SNe Ia from LOWZ, SDSS, and SNLS surveys ($0.1 < z \leq 0.85$), by using two different light-curve fitters of SALT2 and MLCS2k2.

5.1. On the Origin of the Environmental Dependence of SN Ia Luminosity

As shown in Section 4, the luminosity dependence would impact on estimating cosmological parameters. It is therefore important to investigate the origin of the dependence in order to use an SN Ia as a more accurate standard candle.

These remaining trends, after “empirical” light-curve corrections, would indicate that 1) there are intrinsic “physical” processes that we do not understand yet, or 2) we simply require a “third parameter” when we analyze SN Ia light-curves. The latter case was intensively performed by Scolnic et al. (2018).

Scolnic et al. (2018) analyzed the SN light-curves using a modified version of SALT2. As we briefly described in Section 3.2.4, they included two extra terms in their SALT2 analysis: Δ_M and Δ_B , such that

$$\mu_{SN} = m_B - M_B + \alpha \times X_1 - \beta \times C + \Delta_M + \Delta_B, \quad (3)$$

where Δ_M is a distance correction based on the observed trend between SN Ia luminosity and host mass, and Δ_B is another distance correction based on the predicted bias estimated from SN survey simulations (Kessler & Scolnic 2017). Furthermore, they considered distance biases due to intrinsic scatter, introduced

by Scolnic & Kessler (2016). However, after these all extra corrections, they still observed the HR difference of 0.053 ± 0.009 mag (5.9σ , see Table 9). They argued that when they do not include these additional corrections the size of HR difference increases to 0.071 ± 0.010 mag (7.1σ). This result would indicate that the correction with various functional forms is not appropriate to capture the remaining trends in SN Ia luminosity and host galaxy properties. Instead of that, we require the understanding of detailed physics of SNe Ia.

Since the host $M_{stellar}$ and $sSFR$ cannot directly affect the SN luminosity, the theoretical studies suggested that the leading candidates for the observed trends are the progenitor age and the progenitor metallicity (Timmes et al. 2003; Kasen et al. 2009). Both are empirically known to correlate with the host $M_{stellar}$ and $sSFR$ (e.g., Tremonti et al. 2004; Gallazzi et al. 2005; Kang et al. 2016).

In order to explore these issues more directly, there are several studies to deal with the host galaxy age and (gas-phase or stellar) metallicity (e.g., Neill et al. 2009; Sullivan et al. 2010; Gupta et al. 2011; Johansson et al. 2013; Pan et al. 2014; Campbell et al. 2016; Wolf et al. 2016). Most of the studies used the SED fitting technique or emission lines. However, the limitations of those methods, such as the age-metallicity degeneracy and attenuation by dust, are well-known (see Worthey et al. 1994; Walcher et al. 2011). In order to overcome these limitations, Balmer absorption lines have been widely used in estimating the age and the metallicity of early-type galaxies during the last two decades (Faber et al. 1992; Worthey et al. 1994; Worthey 1998; Trager et al. 2000; Thomas et al. 2005; Kuntschner et al. 2006; Graves et al. 2007, 2009; Conroy & Gunn 2010). In the recent study of Kang et al. (2016), they employed Balmer absorption lines to determine more reliable population ages and metallicities for 27 early-type host galaxies. From high signal-to-noise observed spectra (≥ 100 per pixel), they suggested that the stellar population age is mainly responsible for the relation between SN Ia luminosities and host properties at the $\sim 3.9\sigma$ level. Even though more data are required to further confirm this result, this kind of study would provide the direct evidence for the origin of the environmental dependence and the evolution of SN Ia luminosity.

Furthermore, we would suggest another indirect approach to explore the origin of the environmental dependence of SN Ia luminosities in the context of a galaxy. Our results and many previous studies showed that SN Ia luminosity is changed at $\log(M_{stellar}) = 10$ (Section 3.2), and also as mentioned in Section 2.5.1, Kim et al. (2018) method to infer the local environments from the global host properties requires this mass scale. The mass scale of $10^{10} M_{\odot}$ takes on a unique position in galaxy studies. Numerous observational studies found that a transition in the assembly histories of galaxies for both early- and late-types and a transition of galaxy morphology occur near this mass scale (e.g., Kauffmann et al. 2003; Balcells et al. 2007; Hopkins et al. 2009; Cap-

bellari et al. 2013; Bernardi et al. 2014). In addition, several recent simulations predicted another transition between the SN feedback and the AGN feedback at near this mass (e.g., Crain et al. 2015; Bower et al. 2017; Taylor et al. 2017), and those studies are explored by observations (Martín-Navarro & Mezcua 2018). Taken all these studies together, the origin of the luminosity difference in SNe Ia might be related to the suggested transitions. As the average mass, metallicity, and the population age of host galaxies change with these transitions, the SN progenitor properties and environments would also change as well. This, in turn, affects the SN explosion mechanism, and therefore leads to the SN Ia luminosity difference.

5.2. Luminosity Evolution of SNe Ia?

Since the discovery of the accelerating universe, there have been many studies concerning the luminosity evolution of SNe Ia in various ways. At earlier works, most of them used photometric information, such as the host morphology (Riess et al. 1998; Schmidt et al. 1998) and the SN rise time (Riess et al. 1999b). As more and more SN Ia spectroscopic data became available, recent studies compared average spectra at high-redshift with those at low-redshift (Bronder et al. 2008; Foley et al. 2008; Balland et al. 2009; Sullivan et al. 2009). On the theoretical aspects, there are several SN explosion models to study the evolution effects (Höflich et al. 1998; Timmes et al. 2003; Kasen et al. 2009). Interestingly, most of these studies suggested that the size of luminosity evolution effect is ~ 0.2 mag.

In this paper, we suggested that the stellar population age of host galaxies might be the origin of the environmental dependence of SN Ia luminosity. As the mean population age of host galaxies is known to evolve with redshift, the mean luminosity of SNe Ia also would change with redshift. In order to investigate this, we split the YONSEI Cosmology sample into several redshift bins, and calculate the weighted-mean of HRs in each bin. Figure 27 shows the evolution of the mean SNe Ia luminosity with respect to the redshift. We can see a hint of some luminosity evolution even after the standard light-curve corrections and the size of it is < 0.1 mag, which is a smaller value than that suggested in previous theoretical studies (see above paragraph). This is because the light-curve corrections could dilute the luminosity evolution, as the model of light-curve corrections takes an average SN Ia at an average redshift (see Guy et al. 2007). To examine this, we also plot the mean SN Ia luminosity *without* the light-curve corrections with SALT2 and MLCS2k2 in Figure 27. The size of the luminosity evolution *without* the light-curve corrections is larger than that *with* the light-curve corrections: ~ 0.4 mag for the SALT2 sample and ~ 0.2 mag for the MLCS2k2 sample. Interestingly, a trend of the luminosity evolution is similar until the intermediate-redshift range, while at the high-redshift range only the sample *without* the SALT2 light-curve correction shows a different trend. Further data, especially at the high-redshift range, are required to confirm the luminosity

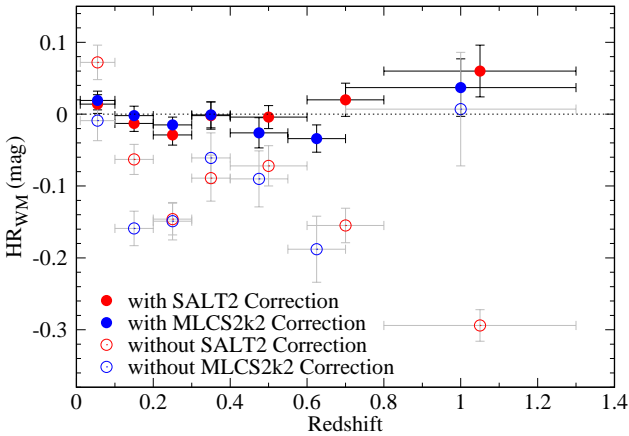


Figure 27. Luminosity evolution of SNe Ia with respect to the redshift. Each data point is the weighted-mean of HRs in each redshift bin from the YONSEI Cosmology sample for SALT2 (red) and MLCS2k2 (blue). Filled circles are the values *with* the light-curve corrections, while open circles are estimated *without* the light-curve corrections. An errorbar in redshift is a bin size. A hint of the luminosity evolution is observed, but further data are required to confirm the luminosity evolution.

evolution of SNe Ia in detail.

In order to investigate the impact of the luminosity evolution of SNe Ia on the cosmological inference, several studies predicted the best-fit cosmological models taking into account a term for the luminosity evolution (e.g., Drell et al. 2000; Linden et al. 2009; Tutusaus et al. 2017, 2018). The latest study of Tutusaus et al. (2018) concluded that a non-accelerated universe was able to correctly fit all the main probes if SN Ia luminosity evolution is allowed. Riess et al. (1999b) mentioned that an unexpected luminosity evolution would be sufficient to nullify the cosmological conclusions. Therefore, in order to confirm whether the luminosity evolution of SNe Ia is important or not, we require more SN data at $z > 1$ (see Figure 27), where the effect of dark energy and the luminosity evolution is distinguishable.

5.3. Future Work

The current data is good enough to put the discussion for the origin and luminosity evolution of SNe Ia on the table, although more observations for SNe Ia and their host galaxies are still required.

Especially, as investigated by Kang et al. (2016) (see Section 5.1), in order to conclude the current issues on the origin of the environmental dependence and the evolution of SNe Ia at the significant confidence level, we need more, at least 100, early-type host galaxies. From ongoing SN surveys at the low-redshift range, such as the Zwicky Transient Facility (Bellm et al. 2019; Graham et al. 2019), the Korea Microlensing Telescope Network (Kim et al. 2016), and the Foundation SN Survey (Foley et al. 2018), plenty of early-type hosts will be taken for obtaining the high signal-to-noise ratio spectra to determine more reliable population ages and metallicities for host galaxies. Furthermore, in the era of

30 m class telescopes, we would expect that we can expand the redshift range to 0.5 or above. The Dark Energy Survey (Flaugher et al. 2015) SN program expects ~ 270 early-type host galaxies to be observed up to the redshift of 1.0. At this high-redshift, a classification of galaxy morphology is another challenge. In order to more reliably select early-type host galaxies in this redshift range, we should develop or improve the method for the galaxy morphology classification, as has done before for the SDSS sample (e.g., Park & Choi 2005; Choi et al. 2010) and the HST Cluster SN Survey sample (see Meyers et al. 2012; Suzuki et al. 2012).

ACKNOWLEDGMENTS

We thank the referees for a number of helpful comments. This work was supported by the National Research Foundation of Korea to the Center for Galaxy Evolution Research through the grant programs No. 2017R1A5A1070354 and 2017R1A2B3002919. Y.-L.K. acknowledges support from the European Research Council (ERC) under the European Unions Horizon 2020 research and innovation programme (grant agreement No. 759194 - USNAC). This research has made use of the NASA/IPAC Extragalactic Database (NED), which is operated by the Jet Propulsion Laboratory, California Institute of Technology, under contract with the National Aeronautics and Space Administration. We acknowledge the usage of the HyperLeda database (<http://leda.univ-lyon1.fr>).

REFERENCES

- Balcells, M., Graham, A. W., & Peletier, R. F. 2007, Galactic Bulges from Hubble Space Telescope NICMOS Observations: Global Scaling Relations, *ApJ*, 665, 1104
- Balland, C., Baumont, S., Basa, S., et al. 2009, The ESO/VLT 3rd Year Type Ia Supernova Data Set from the Supernova Legacy Survey, *A&A*, 507, 85
- Bellm, E. C., Kulkarni, S. R., Graham, M. J., et al. 2019, The Zwicky Transient Facility: System Overview, Performance, and First Results, *PASP*, 131, 018002
- Bernardi, M., Meert, A., Vikram, V., et al. 2014, Systematic Effects on the Size-Luminosity Relations of Early- and Late-Type Galaxies: Dependence on Model Fitting and Morphology, *MNRAS*, 443, 874
- Betoule, M., Kessler, R., Guy, J., et al. 2014, Improved Cosmological Constraints from a Joint Analysis of the SDSS-II and SNLS Supernova Samples, *A&A*, 568, A22
- Bower, R. G., Schaye, J., Frenk, C. S., et al. 2017, The Dark Nemesis of Galaxy Formation: Why Hot Haloes Trigger Black Hole Growth and Bring Star Formation to an End, *MNRAS*, 465, 32
- Bronder, T. J., Hook, I. M., Astier, P., et al. 2008, SNLS Spectroscopy: Testing for Evolution in Type Ia Supernovae, *A&A*, 477, 717
- Campbell, H., D’Andrea, C. B., Nichol, R. C., et al. 2013, Cosmology with Photometrically Classified Type Ia Supernovae from the SDSS-II Supernova Survey, *ApJ*, 763, 88
- Campbell, H., Fraser, M., & Gilmore, G. 2016, How SN Ia Host-Galaxy Properties Affect Cosmological Parameters, *MNRAS*, 457, 3470

- Cappellari, M., McDermid, R. M., Alatalo, K., et al. 2013, The ATLAS^{3D} Project - XX. Mass-Size and Mass- σ Distributions of Early-Type Galaxies: Bulge Fraction Drives Kinematics, Mass-to-Light Ratio, Molecular Gas Fraction and Stellar Initial Mass Function, *MNRAS*, 432, 1862
- Childress, M., Aldering, G., Antilogus, P., et al. 2013, Host Galaxy Properties and Hubble Residuals of Type Ia Supernovae from the Nearby Supernova Factory, *ApJ*, 770, 108
- Childress, M. J., Wolf, C., & Zahid, H. J. 2014, Ages of Type Ia Supernovae over Cosmic Time, *MNRAS*, 445, 1898
- Choi, Y.-Y., Han, D.-H., & Kim, S. S. 2010, Korea Institute for Advanced Study Value-Added Galaxy Catalog, *JKAS*, 43, 191
- Conley, A., Guy, J., Sullivan, M., et al. 2011, Supernova Constraints and Systematic Uncertainties from the First Three Years of the Supernova Legacy Survey, *ApJS*, 192, 1
- Conroy, C., & Gunn, J. E. 2010, The Propagation of Uncertainties in Stellar Population Synthesis Modeling. III. Model Calibration, Comparison, and Evaluation, *ApJ*, 712, 833
- Contreras, C., Hamuy, M., Phillips, M. M., et al. 2010, The Carnegie Supernova Project: First Photometry Data Release of Low-Redshift Type Ia Supernovae, *AJ*, 139, 519
- Crain, R. A., Schaye, J., Bower, R. G., et al. 2015, The EAGLE Simulations of Galaxy Formation: Calibration of Subgrid Physics and Model Variations, *MNRAS*, 450, 1937
- D'Andrea, C. B., Gupta, R. R., Sako, M., et al. 2011, Spectroscopic Properties of Star-forming Host Galaxies and Type Ia Supernova Hubble Residuals in a Nearly Unbiased Sample, *ApJ*, 743, 172
- Drell, P. S., Lored, T. J., & Wasserman, I. 2000, Type Ia Supernovae, Evolution, and the Cosmological Constant, *ApJ*, 530, 593
- Driver, S. P., Andrews, S. K., da Cunha, E., et al. 2018, GAMA/G10-COSMOS/3D-HST: the $0 < z < 5$ Cosmic Star Formation History, Stellar-Mass, and Dust-Mass Densities, *MNRAS*, 475, 2891
- Faber, S. M., Worthey, G., & Gonzales, J. J. 1992, Absorption-Line Spectra of Elliptical Galaxies and Their Relation to Elliptical Formation, The Stellar Populations of Galaxies, 149, 255
- Filippenko, A. V. 1989, Type Ia Supernovae in Elliptical and Spiral Galaxies - Possible Differences in Photometric Homogeneity, *PASP*, 101, 588
- Fioc, M., & Rocca-Volmerange, B. 1997, PEGASE: a UV to NIR Spectral Evolution Model of Galaxies. Application to the Calibration of Bright Galaxy Counts., *A&A*, 326, 950
- Flaugher, B., Diehl, H. T., Honscheid, K., et al. 2015, The Dark Energy Camera, *AJ*, 150, 150
- Foley, R. J., Filippenko, A. V., Aguilera, C., et al. 2008, Constraining Cosmic Evolution of Type Ia Supernovae, *ApJ*, 684, 68
- Foley, R. J., Scolnic, D., Rest, A., et al. 2018, The Foundation Supernova Survey: Motivation, Design, Implementation, and First Data Release, *MNRAS*, 475, 193
- Gallagher, J. S., Garnavich, P. M., Berlind, P., et al. 2005, Chemistry and Star Formation in the Host Galaxies of Type Ia Supernovae, *ApJ*, 634, 210
- Gallagher, J. S., Garnavich, P. M., Caldwell, N., et al. 2008, Supernovae in Early-Type Galaxies: Directly Connecting Age and Metallicity with Type Ia Luminosity, *ApJ*, 685, 752
- Gallazzi, A., Charlot, S., Brinchmann, J., White, S. D. M., & Tremonti, C. A. 2005, The Ages and Metallicities of Galaxies in the Local Universe, *MNRAS*, 362, 41
- Graham, M. J., Kulkarni, S. R., Bellm, E. C., et al. 2019, The Zwicky Transient Facility: Science Objectives, *arXiv:1902.01945*
- Graves, G. J., Faber, S. M., Schiavon, R. P., & Yan, R. 2007, Ages and Abundances of Red Sequence Galaxies as a Function of LINER Emission-Line Strength, *ApJ*, 671, 243
- Graves, G. J., Faber, S. M., & Schiavon, R. P. 2009, Dissecting the Red Sequence. II. Star Formation Histories of Early-Type Galaxies Throughout the Fundamental Plane, *ApJ*, 698, 1590
- Gupta, R. R., D'Andrea, C. B., Sako, M., et al. 2011, Improved Constraints on Type Ia Supernova Host Galaxy Properties Using Multi-Wavelength Photometry and Their Correlations with Supernova Properties, *ApJ*, 740, 92
- Guy, J., Astier, P., Baumont, S., et al. 2007, SALT2: Using Distant Supernovae to Improve the Use of Type Ia Supernovae as Distance Indicators, *A&A*, 466, 11
- Guy, J., Sullivan, M., Conley, A., et al. 2010, The Supernova Legacy Survey 3-Year Sample: Type Ia Supernovae Photometric Distances and Cosmological Constraints, *A&A*, 523, A7
- Hamuy, M., Phillips, M. M., Maza, J., et al. 1995, A Hubble Diagram of Distant Type IA Supernovae, *AJ*, 109, 1
- Hamuy, M., Phillips, M. M., Suntzeff, N. B., et al. 1996a, The Absolute Luminosities of the Calan/Tololo Type IA Supernovae, *AJ*, 112, 2391
- Hamuy, M., Phillips, M. M., Suntzeff, N. B., et al. 1996b, BVRI Light Curves for 29 Type IA Supernovae, *AJ*, 112, 2408
- Hamuy, M., Trager, S. C., Pinto, P. A., et al. 2000, A Search for Environmental Effects on Type IA Supernovae, *AJ*, 120, 1479
- Han, D.-H., Park, C., Choi, Y.-Y., & Park, M.-G. 2010, The Properties of Type Ia Supernova Host Galaxies from the Sloan Digital Sky Survey, *ApJ*, 724, 502
- Hicken, M., Challis, P., Jha, S., et al. 2009a, CfA3: 185 Type Ia Supernova Light Curves from the CfA, *ApJ*, 700, 331
- Hicken, M., Wood-Vasey, W. M., Blondin, S., et al. 2009b, Improved Dark Energy Constraints from ~ 100 New CfA Supernova Type Ia Light Curves, *ApJ*, 700, 1097
- Hicken, M., Challis, P., Kirshner, R. P., et al. 2012, CfA4: Light Curves for 94 Type Ia Supernovae, *ApJS*, 200, 12
- Höflich, P., Wheeler, J. C., & Thielemann, F. K. 1998, Type Ia Supernovae: Influence of the Initial Composition on the Nucleosynthesis, Light Curves, and Spectra and Consequences for the Determination of Ω_M and Λ , *ApJ*, 495, 617
- Hopkins, P. F., Somerville, R. S., Cox, T. J., et al. 2009, The Effects of Gas on Morphological Transformation in Mergers: Implications for Bulge and Disc Demographics, *MNRAS*, 397, 802
- Howell, D. A., Sullivan, M., Brown, E. F., et al. 2009, The Effect of Progenitor Age and Metallicity on Luminosity and ^{56}Ni Yield in Type Ia Supernovae, *ApJ*, 691, 661
- Jha, S., Kirshner, R. P., Challis, P., et al. 2006, UBVRI Light Curves of 44 Type Ia Supernovae, *AJ*, 131, 527

- Jha, S., Riess, A. G., & Kirshner, R. P. 2007, Improved Distances to Type Ia Supernovae with Multicolor Light-Curve Shapes: MLCS2k2, *ApJ*, 659, 122
- Johansson, J., Thomas, D., Pforr, J., et al. 2013, SN Ia Host Galaxy Properties from Sloan Digital Sky Survey-II Spectroscopy, *MNRAS*, 435, 1680
- Jones, D. O., Riess, A. G., & Scolnic, D. M. 2015, *ApJ*, Reconsidering the Effects of Local Star Formation on Type Ia Supernova Cosmology, 812, 31
- Jones, D. O., Scolnic, D. M., Riess, A. G., et al. 2018a, Measuring Dark Energy Properties with Photometrically Classified Pan-STARRS Supernovae. II. Cosmological Parameters, *ApJ*, 857, 51
- Jones, D. O., Riess, A. G., Scolnic, D. M., et al. 2018b, Should Type Ia Supernova Distances Be Corrected for Their Local Environments?, *ApJ*, 867, 108
- Jönsson, J., Sullivan, M., Hook, I., et al. 2010, Constraining Dark Matter Halo Properties Using Lensed Supernova Legacy Survey Supernovae, *MNRAS*, 405, 535
- Kang, Y., Kim, Y.-L., Lim, D., Chung, C., & Lee, Y.-W. 2016, Early-Type Host Galaxies of Type Ia Supernovae. I. Evidence for Downsizing, *ApJS*, 223, 7
- Kasen, D., Röpke, F. K., & Woosley, S. E. 2009, The Diversity of Type Ia Supernovae from Broken Symmetries, *Nature*, 460, 869
- Kauffmann, G., Heckman, T. M., White, S. D. M., et al. 2003, The Dependence of Star Formation History and Internal Structure on Stellar Mass for 10^5 Low-Redshift Galaxies, *MNRAS*, 341, 54
- Kelly, P. L., Hicken, M., Burke, D. L., Mandel, K. S., & Kirshner, R. P. 2010, Hubble Residuals of Nearby Type Ia Supernovae are Correlated with Host Galaxy Masses, *ApJ*, 715, 743
- Kelly, P. L., Filippenko, A. V., Burke, D. L., et al. 2015, Distances with $<4\%$ Precision from Type Ia Supernovae in Young Star-Forming Environments, *Science*, 347, 1459
- Kessler, R., Becker, A. C., Cinabro, D., et al. 2009a, First-Year Sloan Digital Sky Survey-II Supernova Results: Hubble Diagram and Cosmological Parameters, *ApJS*, 185, 32
- Kessler, R., Bernstein, J. P., Cinabro, D., et al. 2009b, SNANA: A Public Software Package for Supernova Analysis, *PASP*, 121, 1028
- Kessler, R., & Scolnic, D. 2017, Correcting Type Ia Supernova Distances for Selection Biases and Contamination in Photometrically Identified Samples, *ApJ*, 836, 56
- Kim, S.-L., Lee, C.-U., Park, B.-G., et al. 2016, KMTNET: A Network of 1.6 m Wide-Field Optical Telescopes Installed at Three Southern Observatories, *JKAS*, 49, 37
- Kim, Y.-L., Kang, Y., & Lee, Y.-W. 2015, Yonsei Nearby Supernova Evolution Investigation (YONSEI) Supernova Catalogue, *PKAS*, 30, 485
- Kim, Y.-L., Smith, M., Sullivan, M., & Lee, Y.-W. 2018, Environmental Dependence of Type Ia Supernova Luminosities from a Sample without a Local-Global Difference in Host Star Formation, *ApJ*, 854, 24
- Kuntschner, H., Emsellem, E., Bacon, R., et al. 2006, The SAURON Project - VI. Line Strength Maps of 48 Elliptical and Lenticular Galaxies, *MNRAS*, 369, 497
- Lampeitl, H., Smith, M., Nichol, R. C., et al. 2010, The Effect of Host Galaxies on Type Ia Supernovae in the SDSS-II Supernova Survey, *ApJ*, 722, 566
- Le Borgne, D., & Rocca-Volmerange, B. 2002, Photometric Redshifts from Evolutionary Synthesis with PÉGASE: The Code Z-PEG and the $z=0$ Age Constraint, *A&A*, 386, 446
- Le Borgne, D., Rocca-Volmerange, B., Prugniel, P., et al. 2004, Evolutionary Synthesis of Galaxies at High Spectral Resolution with the Code PEGASE-HR. Metallicity and Age Tracers, *A&A*, 425, 881
- Linden, S., Virey, J.-M., & Tilquin, A. 2009, Cosmological Parameter Extraction and Biases from Type Ia Supernova Magnitude Evolution, *A&A*, 506, 1095
- Madau, P., & Dickinson, M. 2014, Cosmic Star-Formation History, *ARA&A*, 52, 415
- Makarov, D., Prugniel, P., Terekhova, N., Courtois, H., & Vauglin, I. 2014, HyperLEDA. III. The Catalogue of Extragalactic Distances, *A&A*, 570, A13
- Malmquist, K. G. 1936, The Effect of an Absorption of Light in Space upon Some Relations in Stellar Statistics, *Stockholms Obs. Medd.*, 26
- Martín-Navarro, I., & Mezcua, M. 2018, Exploring the Limits of AGN Feedback: Black Holes and the Star Formation Histories of Low-Mass Galaxies, *ApJL*, 855, L20
- Meyers, J., Aldering, G., Barbary, K., et al. 2012, The Hubble Space Telescope Cluster Supernova Survey. III. Correlated Properties of Type Ia Supernovae and Their Hosts at $0.9 < Z < 1.46$, *ApJ*, 750, 1
- Miknaitis, G., Pignata, G., Rest, A., et al. 2007, The ESSENCE Supernova Survey: Survey Optimization, Observations, and Supernova Photometry, *ApJ*, 666, 674
- Neill, J. D., Sullivan, M., Howell, D. A., et al. 2009, *ApJ*, The Local Hosts of Type Ia Supernovae, 707, 1449
- Pan, Y.-C., Sullivan, M., Maguire, K., et al. 2014, The Host Galaxies of Type Ia Supernovae Discovered by the Palomar Transient Factory, *MNRAS*, 438, 1391
- Park, C., & Choi, Y.-Y. 2005, Morphology Segregation of Galaxies in Color-Color Gradient Space, *ApJL*, 635, L29
- Perlmutter, S., Aldering, G., Goldhaber, G., et al. 1999, Measurements of Ω and Λ from 42 High-Redshift Supernovae, *ApJ*, 517, 565
- Phillips, M. M. 1993, The Absolute Magnitudes of Type IA Supernovae, *ApJL*, 413, L105
- Rest, A., Scolnic, D., Foley, R. J., et al. 2014, Cosmological Constraints from Measurements of Type Ia Supernovae Discovered during the First 1.5 yr of the Pan-STARRS1 Survey, *ApJ*, 795, 44
- Riess, A. G., Filippenko, A. V., Challis, P., et al. 1998, Observational Evidence from Supernovae for an Accelerating Universe and a Cosmological Constant, *AJ*, 116, 1009
- Riess, A. G., Kirshner, R. P., Schmidt, B. P., et al. 1999a, BVRI Light Curves for 22 Type IA Supernovae, *AJ*, 117, 707
- Riess, A. G., Filippenko, A. V., Li, W., & Schmidt, B. P. 1999b, Is There an Indication of Evolution of Type Ia Supernovae from Their Rise Times?, *AJ*, 118, 2668
- Riess, A. G., Strolger, L.-G., Tonry, J., et al. 2004, Type Ia Supernova Discoveries at $z > 1$ from the Hubble Space Telescope: Evidence for Past Deceleration and Constraints on Dark Energy Evolution, *ApJ*, 607, 665
- Riess, A. G., Strolger, L.-G., Casertano, S., et al. 2007, New Hubble Space Telescope Discoveries of Type Ia Supernovae at $z \geq 1$: Narrowing Constraints on the Early Behavior of Dark Energy, *ApJ*, 659, 98
- Rigault, M., Copin, Y., Aldering, G., et al. 2013, Evidence of Environmental Dependencies of Type Ia Supernovae from the Nearby Supernova Factory Indicated by Local $H\alpha$, *A&A*, 560, A66

- Rigault, M., Aldering, G., Kowalski, M., et al. 2015, Confirmation of a Star Formation Bias in Type Ia Supernova Distances and Its Effect on the Measurement of the Hubble Constant, *ApJ*, 802, 20
- Rigault, M., Brinnel, V., Aldering, G., et al. 2018, Strong Dependence of Type Ia Supernova Standardization on the Local Specific Star Formation Rate, arXiv:1806.03849
- Roman, M., Hardin, D., Betoule, M., et al. 2018, Dependence of Type Ia Supernova Luminosities on Their Local Environment, *A&A*, 615, A68
- Sako, M., Bassett, B., Becker, A. C., et al. 2018, The Data Release of the Sloan Digital Sky Survey-II Supernova Survey, *PASP*, 130, 064002
- Schmidt, B. P., Suntzeff, N. B., Phillips, M. M., et al. 1998, The High-Z Supernova Search: Measuring Cosmic Deceleration and Global Curvature of the Universe Using Type Ia Supernovae, *ApJ*, 507, 46
- Scolnic, D., Rest, A., Riess, A., et al. 2014, Systematic Uncertainties Associated with the Cosmological Analysis of the First Pan-STARRS1 Type Ia Supernova Sample, *ApJ*, 795, 45
- Scolnic, D., & Kessler, R. 2016, Measuring Type Ia Supernova Populations of Stretch and Color and Predicting Distance Biases, *ApJL*, 822, L35
- Scolnic, D. M., Jones, D. O., Rest, A., et al. 2018, The Complete Light-Curve Sample of Spectroscopically Confirmed SNe Ia from Pan-STARRS1 and Cosmological Constraints from the Combined Pantheon Sample, *ApJ*, 859, 101
- Smith, M., Nichol, R. C., Dilday, B., et al. 2012, The SDSS-II Supernova Survey: Parameterizing the Type Ia Supernova Rate as a Function of Host Galaxy Properties, *ApJ*, 755, 61
- Stritzinger, M. D., Phillips, M. M., Boldt, L. N., et al. 2011, The Carnegie Supernova Project: Second Photometry Data Release of Low-Redshift Type Ia Supernovae, *AJ*, 142, 156
- Strolger, L.-G., Riess, A. G., Dahlen, T., et al. 2004, The Hubble Higher z Supernova Search: Supernovae to $z \sim 1.6$ and Constraints on Type Ia Progenitor Models, *ApJ*, 613, 200
- Sullivan, M., Le Borgne, D., Pritchett, C. J., et al. 2006, Rates and Properties of Type Ia Supernovae as a Function of Mass and Star Formation in Their Host Galaxies, *ApJ*, 648, 868
- Sullivan, M., Ellis, R. S., Howell, D. A., et al. 2009, The Mean Type Ia Supernova Spectrum Over the Past Nine Gigayears, *ApJL*, 693, L76
- Sullivan, M., Conley, A., Howell, D. A., et al. 2010, The Dependence of Type Ia Supernovae Luminosities on Their Host Galaxies, *MNRAS*, 406, 782
- Sullivan, M., Guy, J., Conley, A., et al. 2011, *ApJ*, SNLS3: Constraints on Dark Energy Combining the Supernova Legacy Survey Three-Year Data with Other Probes, 737, 102
- Suzuki, N., Rubin, D., Lidman, C., et al. 2012, The Hubble Space Telescope Cluster Supernova Survey. V. Improving the Dark-Energy Constraints above $z > 1$ and Building an Early-Type-Hosted Supernova Sample, *ApJ*, 746, 85
- Taylor, J. 1997, *Introduction to Error Analysis* (2nd ed.: Mill Valley, CA: University Science Books)
- Taylor, P., Federrath, C., & Kobayashi, C. 2017, Star Formation in Simulated Galaxies: Understanding the Transition to Quiescence at $3 \times 10^{10} M_{\odot}$, *MNRAS*, 469, 4249
- Thomas, D., Maraston, C., Bender, R., & Mendes de Oliveira, C. 2005, The Epochs of Early-Type Galaxy Formation as a Function of Environment, *ApJ*, 621, 673
- Timmes, F. X., Brown, E. F., & Truran, J. W. 2003, On Variations in the Peak Luminosity of Type Ia Supernovae, *ApJL*, 590, L83
- Trager, S. C., Faber, S. M., Worthey, G., & González, J. J. 2000, The Stellar Population Histories of Local Early-Type Galaxies. I. Population Parameters, *AJ*, 119, 1645
- Tremonti, C. A., Heckman, T. M., Kauffmann, G., et al. 2004, The Origin of the Mass-Metallicity Relation: Insights from 53,000 Star-Forming Galaxies in the Sloan Digital Sky Survey, *ApJ*, 613, 898
- Tripp, R. 1998, A Two-Parameter Luminosity Correction for Type Ia Supernovae, *A&A*, 331, 815
- Tutusaus, I., Lamine, B., Dupays, A., & Blanchard, A. 2017, Is Cosmic Acceleration Proven by Local Cosmological Probes?, *A&A*, 602, A73
- Tutusaus, I., Lamine, B., & Blanchard, A. 2018, Model-Independent Cosmic Acceleration and Type Ia Supernovae Intrinsic Luminosity Redshift Dependence, arXiv:1803.06197
- Uddin, S. A., Mould, J., Lidman, C., Ruhlmann-Kleider, V., & Zhang, B. R. 2017, The Influence of Host Galaxies in Type Ia Supernova Cosmology, *ApJ*, 848, 56
- Walcher, J., Groves, B., Budavári, T., & Dale, D. 2011, Fitting the Integrated Spectral Energy Distributions of Galaxies, *Ap&SS*, 331, 1
- Wolf, R. C., D'Andrea, C. B., Gupta, R. R., et al. 2016, SDSS-II Supernova Survey: An Analysis of the Largest Sample of Type Ia Supernovae and Correlations with Host-Galaxy Spectral Properties, *ApJ*, 821, 115
- Wood-Vasey, W. M., Miknaitis, G., Stubbs, C. W., et al. 2007, Observational Constraints on the Nature of Dark Energy: First Cosmological Results from the ESSENCE Supernova Survey, *ApJ*, 666, 694
- Worthey, G., Faber, S. M., González, J. J., & Burstein, D. 1994, Old Stellar Populations. 5: Absorption Feature Indices for the Complete LICK/IDS Sample of Stars, *ApJS*, 94, 687
- Worthey, G. 1998, Abundance Ratio Trends and Nucleosynthesis in Elliptical Galaxies and Spheroids, *PASP*, 110, 888